Scanning Microscopy

Volume 8 | Number 3 Article 15

4-25-1994

Multivariate Statistical Analysis Applied to X-Ray Spectra and X-Ray Mapping of Liver Cell Nuclei

Carmen Quintana
INSERM

Noël Bonnet
Université de Reims

Scanning Microscopy, Vol. 8, No. 3, 1994 (Pages 563-586) 0891-7035/94$5.00+.25
Scanning Microscopy International, Chicago (AMF O'Hare), IL 60666 USA

MULTIVARIATE STATISTICAL ANALYSIS APPLIED TO X-RAY SPECTRA AND X-RAY MAPPING OF LIVER CELL NUCLEI

Carmen Quintana[1,2*] and Noël Bonnet[3]

[1]INSERM, France and [2]Centro Nacional de Microelectrónica, CSIC, Madrid, Spain
[3]Université de Reims and INSERM U314, 51100 Reims, France

(Received for publication August 23, 1993, and in revised form April 25, 1994)

Abstract

Principal Components Analysis (PCA) and Factorial Analysis of Correspondence (FAC), two Multivariate Statistical Analyses (MSA), were applied to the analysis of X-ray data. MSA are descriptive methods which graphically display the correlations and anticorrelations between a large number of elements. Series of X-ray spectral data and X-ray maps obtained from rat liver were analyzed with reference to the diffusible elements Na, Mg, Cl, K and Ca and also P and S.

By using an *in situ* precipitation method, the pyroantimonate method, it was found that the free, precipitable cations Na^+, Mg^{2+}, and Ca^{2+} are, in the nuclei, mainly distributed throughout the nucleoplasm. Images obtained from FAC allow those areas rich in nucleic acids to be displayed as areas with a strong anticorrelation between P and Sb.

In cryoprocessed tissues, the evaluated wet mass-fraction of diffusible elements corresponds to physiological values of *total* amounts (free and complexed). PCA makes it possible to graphically display the correlation between P and K in chromatin and nucleolus, the correlation between K, Cl and S in cytoplasm and nucleoplasm and the observation of two populations of nuclei according to different Na, Mg and K concentrations. Factorial images obtained from FAC allow those areas rich in nucleic acids to be displayed as areas with a strong correlation between P and K. Similarly those areas rich in proteins are displayed as areas with a strong correlation between S and K.

Key Words: Multivariate statistical analysis, X-ray mapping, diffusible elements, cell nuclei, cryomethods (cryofixation, freeze-substitution, cryoembedding), pyroantimonate precipitation method, rat liver.

*Address for correspondence:
C. Quintana
Centro Nacional de Microelectrónica, Serrano 144, 28006 Madrid, Spain

Phone Number: 34.1.5625311
FAX Number: 34.1.4117651

Introduction

The analysis of microanalytical results obtained for a large number of elements studied over a large number of biological compartments is not an easy task. This is true for spectroscopy but even for maps since the image quality (contrast, signal-to-noise ratio) is often such that an objective interpretation of the relative concentration of different elements is rather difficult.

We have already emphasized the usefulness of Multivariate Statistical Analysis (MSA) to explore the correlation (and anticorrelation) in X-ray spectroscopy processed data (Quintana and Ollacarizqueta, 1989; Quintana, 1991). The anticorrelation between P and the set of elements S, Al and Zn was shown in different nuclear compartments. However, the way of preparing samples (chemical fixation, progressive lowering of temperature (PLT) dehydration method and Lowicryl HM20 or K4M cryoembedding) prevent us from analyzing diffusible elements.

MSA is not limited to series of data such as concentrations but may also be applied directly to experimental series, like spectra or image series. For instance, MSA has previously been applied to time dependent spectroscopy (Bonnet *et al.*, 1991), to electron energy filtered image series (Hannequin and Bonnet, 1988; Trebbia and Bonnet, 1990; Trebbia and Mory, 1990; Bonnet and Trebbia, 1992) and to X-ray spectroscopic images (King *et al.*, 1989; Paque *et al.*, 1990).

In this work, we applied X-ray microanalysis and MSA to study the distribution of diffusible and non diffusible elements in nuclei of rat hepatic cells.

It is already known that diffusible elements, such as Na, Mg, Cl, K and Ca, may be found in cells either free in the aqueous medium or combined with macromolecules (to form a complex). Free ions play a very important role in several metabolic processes but for some of them their concentrations are very weak in comparison to the total concentrations.

The analysis of diffusible elements must be done on cryoprepared specimens in order to avoid the loss and redistribution of these elements between the different cellular compartments. On cryoprocessed specimens,

the distribution of these elements can be observed and quantified by physical methods such as X-ray microanalysis (XRMA), electron energy loss spectrometry (EELS) and secondary ion mass spectrometry (SIMS). However, these methods provide the measurement of **total** quantities or concentrations of these elements. They do not allow the identification of whether they are free or combined. Therefore, *in situ* physical microanalyses on cryoprepared samples are not adequate for the study of metabolic processes in which the free diffusible elements are involved. This may be done by using other techniques as for example the combination of free Ca^{2+} with colored or fluorescent complexes, where the distribution of free Ca^{2+} in cells can be observed in the light microscope. At the subcellular level, cytochemical methods may be used for the visualization of the distribution of free or weakly bound cations. The potassium pyroantimonate (PA) precipitation method is one of these methods used in electron microscopy. This PA method introduced by Komnick (1962) and optimized by Mentré and Escaig (1988), allows the visualization of free or weakly bound sodium and calcium. Pyroantimonate forms opaque precipitates with Na^+ and Ca^{2+} at the concentrations in the same range as the usual cell concentration, 10^{-2} M Na^+ and 10^{-6} M Ca^{2+}. Subsequent microanalysis is required for the identification of the cation which has been made to precipitate by the pyroantimonate.

For the present study, we have used two preparation methods of the same samples, hepatic tissues: the PA precipitation method according to Mentré and Escaig (1988), and cryomethods (cryofixation, cryosubstitution and cryoembedding). Recently, we have shown that this set of cryomethods provides results similar to those obtained from freeze-dried cryosections (Quintana, 1993). These three cryomethods offer the advantage of a better ultrastructure which is a necessary condition for microanalysis at subcellular level.

The main goals of the present study were:

(1) to check the validity of the PA method for the study of the distribution of the free or weakly bound sodium and calcium elements within the cellular nuclei; and

(2) to discuss the advantages and possibilities for the use of the MSA in order to achieve objective results concerning the correlations (or anticorrelations) between the diffusible and the structural elements P and S at subcellular level.

Materials and Methods

Cryomethods

Cryofixation of liver fragments of about 1 mm^3 from anaesthetized rat was performed by rapid immersion in liquid propane in a home-made device (Halpern and Quintana, 1989; Quintana, 1991). For freeze-substitution and Lowicryl HM23 cryoembedding, we have used a new home-made cryosystem (Quintana, 1992, 1993, 1994). The main characteristics of this integrated cryosystem are:

(1) the cold source is a freezer (minimal temperature 180 K). Cryogenic fluids are not required;

(2) efficient shaking of samples in freeze-substitution and cryoinfiltration liquids;

(3) easy manipulation of samples between the different modules of work;

(4) control of temperature throughout the successive steps, especially during cryopolymerisation; and

(5) total protection from toxic vapors coming from Lowicryl resins.

Freeze-substitution was performed at 183 K for 3 days in pure acetone. The cryoembedding procedure was as follows:

Infiltration: resin-acetone 1:1 (v/v),193 K, 4 hours;
resin-acetone 2:1 (v/v),193 K, 4 hours;
pure resin 193 K, 4 hours;
pure resin 193 K, overnight

Cryopolymerisation was carried out in open flat embedding moulds under UV and an inert N_2 atmosphere, for 4 days. The freezer was then switched off and the blocks were allowed to warm at room temperature under UV radiation for about 2 days. For X-ray microanalysis dry-cut sections (about 1 μm thick) were obtained using glass knives and were spread on Ni grids without any solvent.

Pyroantimonate method

Fragments of rat liver were fixed for 2 hours at 4°C with the following solution: 4% potassium pyroantimonate (Merck), 2% paraformaldehyde, 0.04 M potassium phosphate buffer, 1% phenol; final pH: 7.8. The specific procedures have been described in detail by Mentré and Escaig (1988). After fixation, the tissue was rapidly rinsed in distilled water and dehydrated in a graded series of ethanol. Ethanol was replaced with propylene oxide and embedding was in Araldite. Conventional sections of 0.1-1 μm were obtained using glass knives. Deionized (18 MΩ) water collected in a plastic vessel was used to float sections on the knife trough.

X-ray microanalysis

Energy-dispersive X-ray spectra (EDS) and X-ray maps were recorded at 200 kV in several analytical electron microscopes. The characteristics for the three analytical microscopes are summarized in Table 1. X-ray counts were made over a counting time of 100 sec, in the fixed probe or in the scanning mode.

Treatment of individual X-ray spectra (see also Appendix 1 and 2). The X-ray emission spectra were treated in the following way:

Table 1. Characteristics of the analytical electron microscopes used.

	TEM/STEM Hitachi 800	TEM JEM 2000FX	TEM/STEM Philips CM20
Voltage (kV)	200	200	200
electron source	tungsten	tungsten	LaB_6
d_s(nm)	20-400	100-400	14-19
EDS	Quantum UTW	Link UTW	Quantum UTW
X-ray detector	10 mm^2 $\alpha = 0°$ $\beta = 68°$ $\Omega = 0.011$	10 mm^2 $\alpha = 0°$ $\beta = 70°$ $\Omega = 0.020$	30 mm^2 $\alpha = 90°$ $\beta = 40°$ $\Omega = 0.16$
cold stage	No	No	Yes (113 K)
X-ray analyzer	Microanalyst Kevex 8000	AN10000 Link	AN10000 Link

α = azimuth angle, β = take-off angle, Ω= solid angle, d_s = diameter of the probe; UTW = ultra-thin window.

Table 2. X-ray mapping conditions.

	TEM/STEM Hitachi 800	TEM/STEM Philips CM20
pixels	256 * 128	128 * 128
time/pixel	50 ms	10 ms
n frames	1	8-14

(1) subtraction of continuum X-ray background by using a model based on Kramer's law. (Microanalyst 8000 Kevex system) or by a least-squares fit to filtered profiles method (Link AN10000 system);

(2) deconvolution of the Kα line from Ca and Lα line for Sb or Kß line for K with a Gaussian method (Microanalyst 8000 Kevex system) or with the least-squares fit to filtered profiles method (Link AN10000 system), (see Appendix 2);

(3) semi-quantitative analysis by the standardless method of Cliff and Lorimer (1975). The Quantify/ Foil/Asap analysis with theoretical K-factors in the Microanalyst 8000 Kevex system and the RTS-2/FLS routine in the Link AN10000 system (Appendix 1) were used.

The relative mass-fractions of different analyzed elements may be obtained by this method and compared with those obtained by other authors (Quintana, 1993; 1994).

X-ray mapping

The number of pixels and time per pixel were selected depending on the features of the software used and of the samples stability. The beam current was selected so that the signal-to-noise ratio (S/N) was optimal with a dead time on the detector lower than 50%. The X-ray mapping conditions are summarized in Table 2.

The images for the continuum X-ray background were registered in the spectral region between the Cl and the K peaks (ΔE=3.1-2.8 keV). These images were subtracted pixel by pixel from images of elements O, P, S, K and Sb.

Processing of individual images

Due to the limited integration time, X-ray maps are often characterized by a low S/N. When S/N is less than one, the interpretation of such images becomes less objective. An improvement of S/N can be obtained by digital filtering (low-pass) methods, but this is at the expense of resolution. New methods have now been devised which may improve S/N without too much deterioration of the resolution (Bonnet, unpublished results). We have processed X-ray images according to a variant (Vautrot *et al.*, in preparation) of the anisotropic diffusion method. The aim of this method is to smooth the image within homogeneous regions of the image, but also to avoid averaging within regions containing, e.g., small details or edges. These results (which preserve resolution) can be obtained by iteratively smoothing the image with diffusion functions relying on the image gradient (diffusion is not allowed through a region boundary).

According to the same approach (i.e., local processing instead of global processing), efficient methods of contrast enhancement can be developed and used for improving the display and study of images obtained with cryoembedded sections, where contrast without staining is very weak. In this study, we have used a variant of the contrast enhancement method, in which the local contrast is computed first, then amplified and the grey level resulting from this new value of the contrast is finally computed.

Multivariate Statistical Analysis

Multivariate Statistical Analysis (MSA) refers to a set of methods which were developed by statisticians in order to extract the different pieces of significant information contained in large and possibly complex data sets which can be represented as matrices. These matrices can be understood as representing the content of several

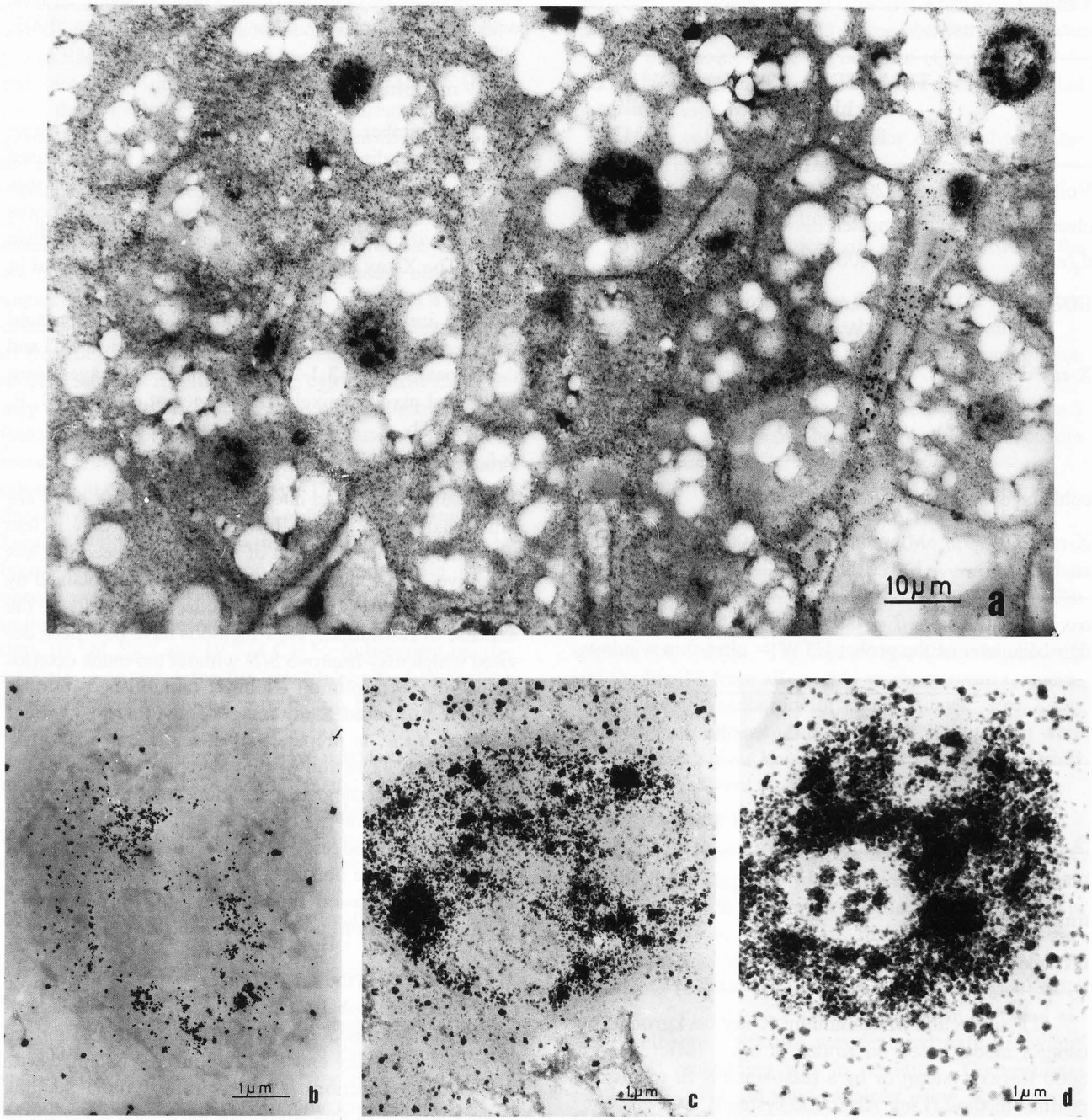

Figure 1. Rat hepatic tissues prepared by the pyroantimonate cation precipitation method. (**a**) View of a group of cells. Note the presence of precipitates in the inter-cellular spaces, in the cytoplasm and in the nuclei. In the nuclei it is possible to distinguish different "patterns" of precipitates. (**b**) Detail of one nucleus containing few small precipitates in the nucleoplasm. The condensed chromatin, the nucleolus and some regions of the nucleoplasm do not contain precipitates. (**c**) Detail of one nucleus containing a large number of precipitates in the nucleoplasm. In some nucleoplasmic areas, the precipitates are grouped in big clusters. (**d**) Detail of one nucleus from about 1 μm thick sections. The nucleolus has a "pattern" of precipitates similar to those of the argyrophilic proteins (see text).

---

variables for different individuals. Therefore, the aim of the method is to describe the interdependence between variables as well as the interdependence between individuals (Benzecri, 1978; Lebart *et al.*, 1979; Foucard, 1982).

In the basic version of MSA, this is done according

to the hypothesis that the global information can be considered as a linear combination of a limited number of pieces of "basic" information, these different pieces being orthogonal (i.e., uncorrelated). This decomposition is obtained through the diagonalization of the so-called variance-covariance matrix of the original data set, thus generating a set of eigenvalues which represent the importance of the information associated with them. To each eigenvalue (ordered by decreasing values) is linked an eigenvector, which can be understood as a new axis of representation for the data set. The whole set of factorial axes generates a vectorial space. The set of factorial axes corresponding to the "most important" eigenvalues generates a subspace where the interpretation of the data set is in general easier than in the original representation space (variables, individuals). This interpretation is made possible by projecting the original data set onto the new space defined by the eigenvectors, i.e., by computing the new coordinates of variables as well as of individuals. Graphical display of these individuals and variables in the factorial planes formed by the two factorial axes (e.g., 1 and 2; 1 and 3) facilitates this interpretation: for instance, two variables which are projected close together in the dominant factorial plane (1-2) can be interpreted as highly correlated regarding the information described by these two axes. Two individuals, which are far from each other when projected onto a factorial plane, can be interpreted as anti-correlated with respect to the information conveyed by these factorial components.

In this paper, MSA was first applied to data sets deduced from X-ray spectra, i.e., to elemental concentrations obtained by processing a series of spectra (variables) recorded in different cellular compartments (individuals). The aim was to consider all the biological compartments simultaneously, instead of computing statistical tests on pairs of elements or pairs of compartments.

For this, we choose one variant of MSA, the Principal Component Analysis (PCA). This analysis was performed with the STATITCF software running on a personal computer. The results of the analysis displayed as tables indicating coordinates of the different elements onto the principal axes (this is the denomination of the factorial axes when PCA is used) and as two-dimensional plots (axes 1 and 2; axes 1 and 3) of the variable and individual coordinates. In the latter case, individuals belonging to different compartments are represented by different symbols. From the study of the relative position of individuals and variables in several planes, it is then possible to induce the correlations between groups of individuals and between groups of variables.

Though originally developed for "small" data matrices resulting from a set of measurements (i.e., spectra processing), MSA can also be applied to the experimental data themselves (spectra, images) provided they can be put in the form of data matrices. This is the case when series of spectra (as a function of time, or at different locations within the specimen) or series of images (as a function of energy, or several images of the same area) are recorded. In this paper, we have also applied MSA to series of different X-ray maps recorded (simultaneously) at a given position on the sample. The aim, again, is to study the relationships between different elements and between different cellular compartments.

A series of N images (e.g., X-ray maps of N elements) constitutes a data set in a N-dimensional space. One trick for analyzing such a large data set consists of finding a reduced M-dimensional space ($M < N$) so that the data set may be more easily interpreted. This is exactly what may be done by one of the variants of MSA, i.e., Principal Component Analysis (PCA), Factorial Analysis of Correspondence (FAC), or Karhunen-Loëve Analysis (KLA). The only difference compared to such an analysis applied to simple results of measurements is that the number of individuals, n, is greater (16384 for a 128 * 128 maps). Otherwise, the steps of the analysis are similar:

(1) Build a matrix, Y(i,j), with the normalized experimental data, where: j = X-ray map number, i = pixel number, and Y = number of counts for pixel i of map j.

(2) Build the variance-covariance matrix, $S = Y^t.Y$, where t means the transposed matrix.

(3) Perform the eigenvalue-eigenvector decomposition of the variance-covariance matrix. The first eigenvectors thus form a new orthogonal basis for the representation of the data set. The X-ray maps may then be represented by their coordinates on the different axes (eigenvectors), and mapping these coordinates on the plane defined by two of these axes helps to visualize the correlations or anticorrelations between the different elements. The image pixels may also be represented by their coordinates on the factorial axes. When these coordinates are converted into grey levels, they may be displayed as factorial images (F1, F2). One may then visualize regions of the object which are responsible for the main sources of information in the original data set.

MSA on X-ray maps was performed with homemade software running on a SUN-4 workstation.

Results

Liver treated by potassium pyroantimonate

Distribution of precipitates. In nuclei of liver hepatocytes we found many different distribution "patterns" of precipitates (Figs. 1a-1d). Some nuclei contain a high number of precipitates while others contain very

Table 3. PCA. Variable analysis.

	Axis 1 (54.1%)	Axis 2 (16.6%)	Axis 3 (13.1%)
Sb	0.9301	-0.1961	0.2377
K	0.7795	0.0949	-0.2855
Na	0.3529	0.6647	-0.5538
P	-0.9210	0.0914	-0.1401
S	-0.8569	0.2316	-0.1326
Ca	-0.7725	-0.2837	-0.0140
Mg	-0.0858	0.7305	0.6590

Correlation between the variables and the main axis. The contribution to the total variance from each axis is indicated in parentheses. 97 points were analyzed.

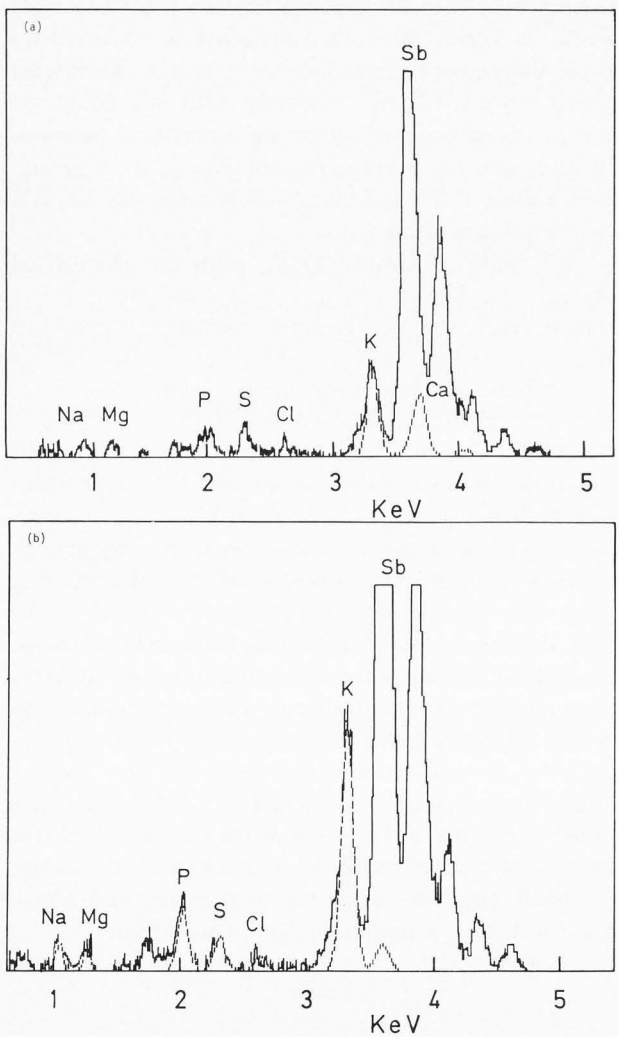

Figure 2. Rat hepatic tissues prepared by the pyroantimonate cation precipitation method. Energy dispersive X-ray spectra of the intranuclear precipitates. The precipitates contain Na, Mg, P, S, K, Ca and Sb (**a**). Some of them do not contain Ca (**b**).

few. The condensed chromatin does not contain any precipitate, although the nucleolus sometimes contains very few and small precipitates. Some precipitates may be also observed in thick sections (around 1 μm) from fibrillar centers (Fig. 1d). There are also precipitates within intercellular areas and in the cytoplasm of some cells. The Sb "stains" the glycogen in some cells (Mentré, 1989).

X-ray Microanalysis. Wavelength dispersive (WDS) X-ray analysis has shown the presence of sodium and calcium in the intra-nuclear precipitates of liver cells (Mentré, 1989). Our present energy dispersive (EDS) X-ray microanalysis shows that the PA precipitates contain Na and Ca, and also Mg and K, which is the cation with the highest concentration in the precipitates. The Ca concentration in certain intranuclear precipitates is lower than the minimum concentration which may be detected in our experimental conditions (Fig. 2).

High Ca quantities may be observed within compartments in which there are no precipitates (condensed chromatin and nucleolus).

MSA over a set of X-ray spectra

Principal components analysis (PCA) was performed over a set of 97 measurements obtained from intranuclear and extranuclear precipitates (cytoplasm and intercellular areas) and over the condensed chromatin and the nucleolus. The outcome of the analysis is shown in Table 3 and Figure 3. We observed:

(1) the correlation between Sb, K, (and Na) in axis 1;

(2) the correlation between P, S, Ca in axis 1,

(3) the anticorrelation between the group of elements (Sb, K, Na) and (P, S, Ca) in axis 1,

(4) the correlation between Na and Mg in axis 2 and the anticorrelation in axis 3.

Axis 1 (which contains more than half of the information) can therefore be interpreted as representing the opposition between the (Sb, K and Na) element group and the (P,S and Ca) element group.

Axis 2 represents the opposition between the (Na, Mg) element group and the (Sb, Ca).

The analyzed areas in plane 1-2 may be divided into 3 groups, G1, G2, G3. Group G1 contains the measurements over the intranuclear areas (●) with either no precipitates at all or very few of them, morphologically identified as chromatin and nucleolus. Group G2 and group G3 are formed by measurements over the precipitates. G2 is essentially formed by the intranuclear precipitates (★); G3 is formed by the intra- and extranuclear precipitates (★ and ■). Group 1 is the richest in P, S and Ca and Group G2 and G3 are the richest in Sb, K and Na. G2 is richer in Na than G3. The mean values for the concentrations in each group calculated according to equation (6) of Appendix 1, are shown in

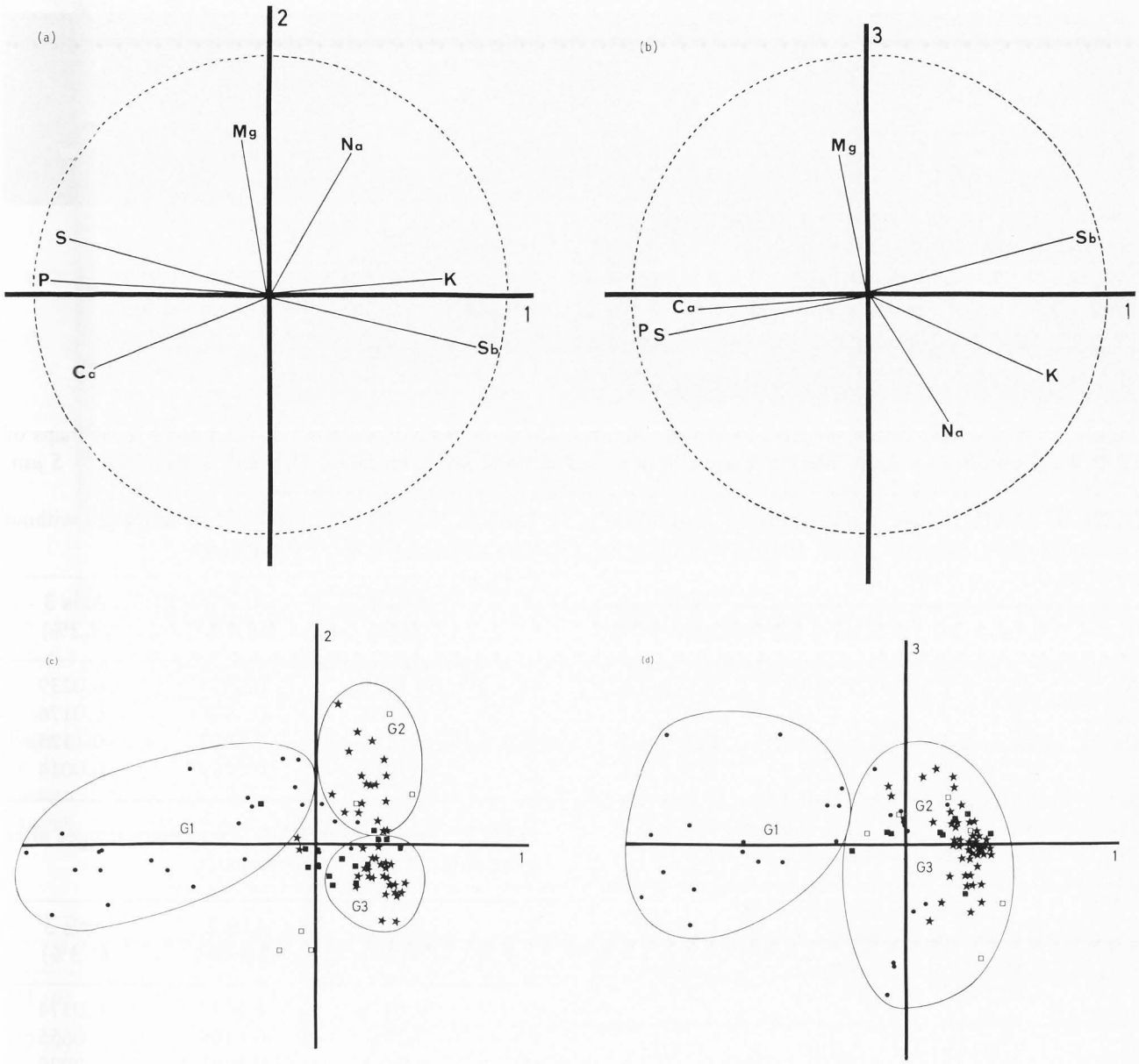

Figure 3. Rat hepatic tissues prepared by the pyroantimonate cation precipitation method. Results of PCA on a set of 97 points analysed from intra and extra-nuclear precipitates, condensed chromatin, nucleolus and glycogen areas. Variables representation; (a) axes 1 and 2; (b) axes 1 and 3. Individuals representation; (c) axes 1 and 2; (d) axes 1 and 3. (●) areas from condensed chromatin, (★) areas from intranuclear precipitates, (■) areas from extra-nuclear precipitates, (□) glycogen areas.

Table 4.

MSA on X-ray maps. The outcome (coordinates of the different elements on the first factorial axes) from the Factorial Analysis of Correspondence over a first series of images from O, P, S, Sb and K and Factorial images over axis 1 (F1) is shown in Table 5 and Figure 4.

We observed as before:

(1) the correlation between Sb and K;

(2) the correlation between P and S; and

(3) the anticorrelation between the group Sb, K and the group P and S.

Axis 1 represents the opposition between Sb, K and P, S, and O. Figure 4 shows images from O, P, K, S, Sb and the corresponding factorial images F1 and F2. The factorial image, F1, represents the strong correlation between Sb and K which separates the regions containing precipitates from the rest of the image. For this image, and throughout the rest of the paper, dark grey

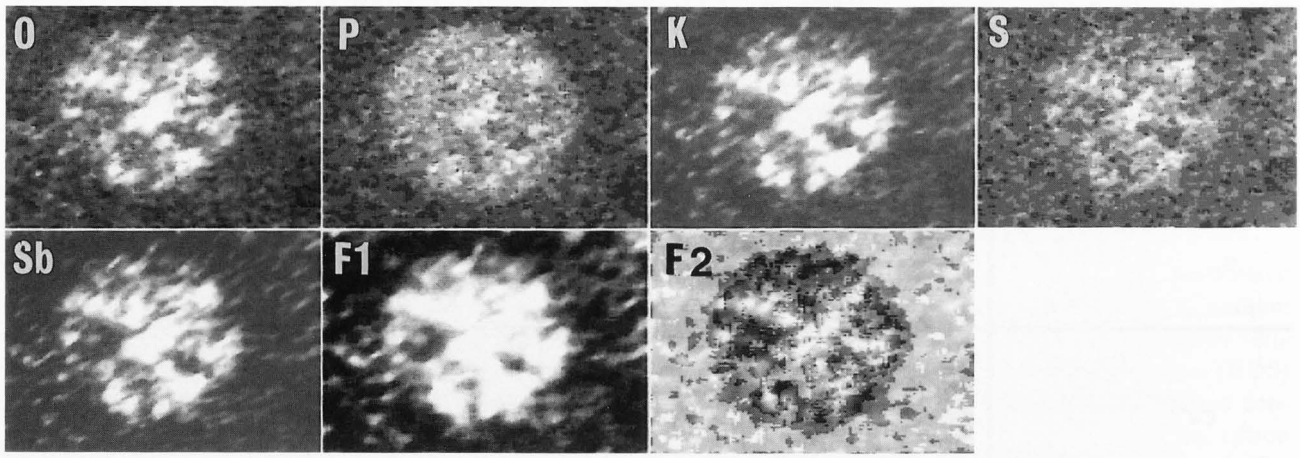

Figure 4. Rat hepatic tissues prepared by the pyroantimonate cation precipitation method. Elemental X-ray maps of O, P, K, S and Sb after local filtering image treatment and factorial image on axes 1 (F1) and 2 (F2). Bar = 5 μm.

Table 4. Cliff-Lorimer semiquantitative analysis of concentration of elements. Mass fraction according to equation (6) in appendix 1.

	G1 (n = 36)	G2 (n = 32)	G3 (n = 24)
Na	2.5 ± 0.7	5.9 ± 0.6	1.1 ± 0.1
Mg	2.0 ± 0.3	2.2 ± 0.2	1.5 ± 0.1
P	28.8 ± 3.5	4.5 ± 0.5	6.2 ± 1.3
S	8.9 ± 0.8	2.1 ± 0.3	2.3 ± 0.5
K	4.5 ± 0.6	8.0 ± 0.3	10.6 ± 0.4
Ca	9.4 ± 1.8	2.9 ± 0.4	1.7 ± 0.3
Sb	44.2 ± 4.6	74.6 ± 0.9	76.6 ± 1.9

Table 5. Results from FAC.

	Axis 1 (72.2%)	Axis 2 (16.4%)	Axis 3 (9.5%)
O	-0.2641	0.0708	0.1160
P	-0.0506	-0.2936	-0.0328
S	-0.1720	0.1321	-0.2194
Sb	0.6242	0.0553	0.0221
K	0.4707	0.0568	0.0311

Correlation between the variables and the main axes. The contribution to the total variance from each axis is indicated in parentheses. 16384 pixels were analyzed.

---

levels represent negative coordinates on the factorial axes and light grey levels represent positive coordinates. Therefore, only the image from K has been included within the following analysis, due to the equivalence between Sb and K distributions.

The effect of the X-ray continuum image subtraction

Table 6. Results from FAC. Element images without subtraction of the X-ray continuum.

	Axis 1 (85%)	Axis 2 (10.7%)	Axis 3 (4.2%)
O	-0.1288	0.0377	0.0239
P	-0.0884	-0.1967	0.0176
S	-0.1113	0.0053	-0.1125
K	0.3212	0.0069	0.0014

Table 7. Results from FAC. Elementary images after subtraction of the X-ray continuum.

	Axis 1 (71.9%)	Axis 2 (20.7%)	Axis 3 (7.3%)
O	0.1473	0.0677	-0.0374
P	0.2991	-0.6109	-0.0655
S	0.2614	-0.0181	0.2970
K	-0.4325	-0.0294	0.0123

in the MSA results, was studied in a second series of images (Tables 6 and 7, and Fig. 5). Figure 5 shows a series of O, P, S and K maps and the factorial F1, F2 and F3 images, before and after X-ray continuum subtraction. The effect of this subtraction is very important in P and S images. This effect is less important in the factorial images; the results are quantitatively similar and only the importance of P within axis 2 increases after the X-ray continuum background subtraction.

In the same way as before, F1 separates those areas which contain the precipitates (nucleoplasm) from the rest of the image. F2 separates those regions with a high content of P (condensed chromatin and nucleolus)

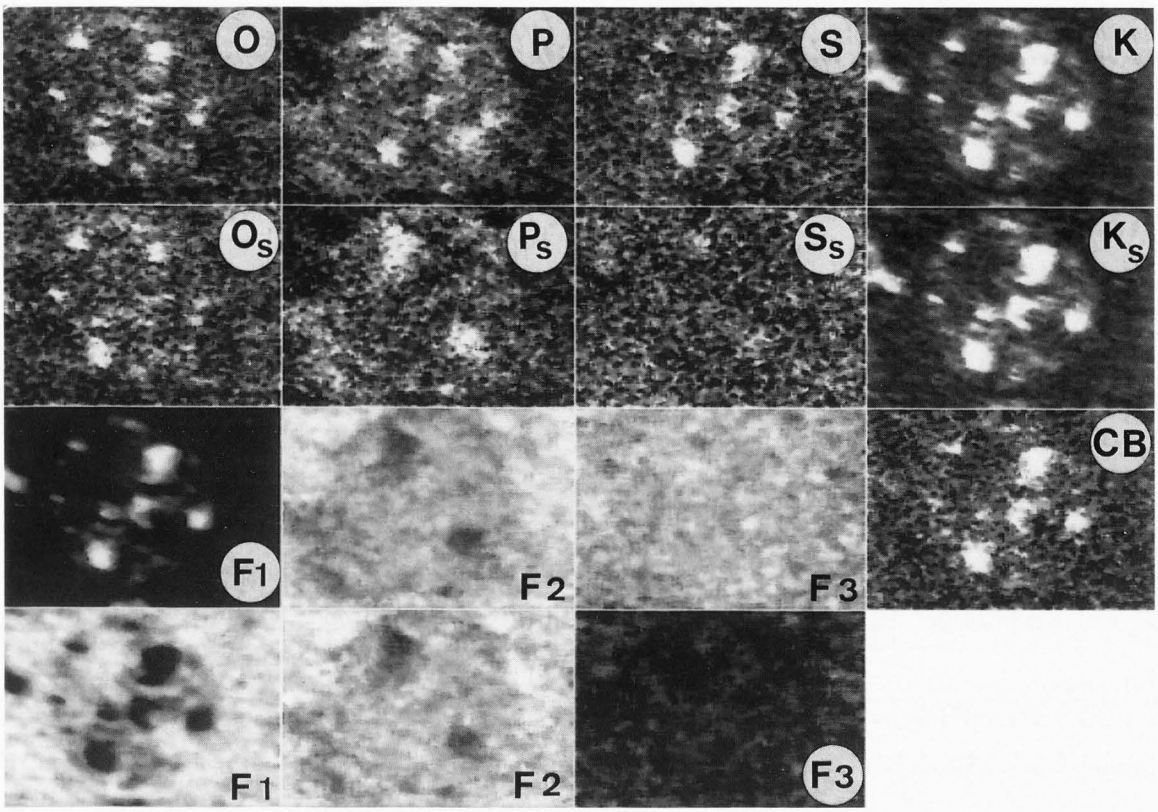

Figure 5. Rat hepatic tissues prepared by the pyroantimonate cation precipitation method. Elemental X-ray maps of O, P, S and K, continuum backgroud (CB) and factorial images F1, F2, F3 before and after X-ray continuum background image subtraction (Os, Ps, Ss, Ks). The important effect of the continuum subtraction on the P and S images can be observed. This effect is less important in the factorial images (see text). Bar = 5 μm.

Table 8. Evaluation of the wet mass fraction.

	Na	Mg	P	S	Cl	K	Ca
N1 (6)	2.5±0.2	2.3±0.2	50±2	15±1	4±0.4	25.6±0.2	0.5±0.1
N2 (3)	2.8±0.5	2±0.2	48±2	15±2	5.5±0.6	26±0.3	0.5±0.1
N3 (4)	0.9±0.3	1.1±0.2	45±2	15±0.5	8±0.6	29±1	0.5±0.2
N4 (4)	9±1	3.6±0.6	44±3	17±2	8±0.6	18±1	0.5±0.2
N5,6 (36)	5±2	3±1	47±4	14±3	7±2	22±3	0.6±0.4

Concentration mean values (* 10^4) (± standard deviation of the mean) in the different analyzed nuclei (N1 to N6). The number of measurements is shown in parentheses.

from the rest. F3 displays a random behavior and cannot be easily interpreted. Figure 6 shows the results from applying FAC over one series of images of the same nucleus acquired with a higher magnification.

In conclusion, we may say that F1 images mainly represent the distribution of the free precipitable cations within the nuclei and F2 images mainly represent the distribution of the nucleic acids. In this case, we can say that the four original maps can be interpreted through the two factorial images (F1 and F2) together with the 8 coordinates of the 4 elements on axes 1 and 2 (Tables 6 and 7). These 2 factorial axes concentrate 92% of the total information. The remaining 8% can be considered as noise.

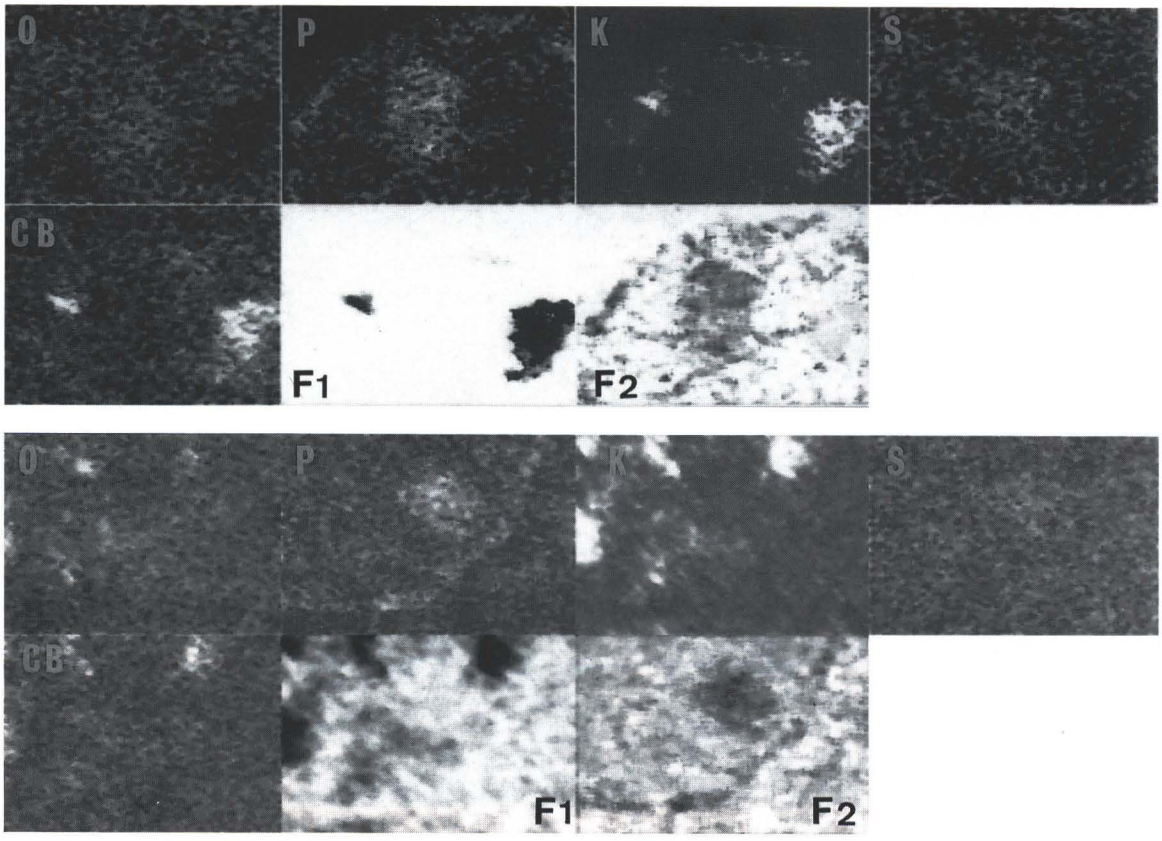

Figure 6. Rat hepatic tissues prepared by the pyroantimonate cation precipitation method. Images of the same nucleus analyzed in Fig. 5 acquired at larger magnification, x 1000. The factorial F1 images represent the free cation distribution in the nucleoplasm. The factorial F2 images represent the P distribution in nucleic acids (condensed chromatin and nucleolus).

Table 9. Results from PCA

	Axis 1 (40.1%)	Axis 2 28.7%)	Axis 3 (12.5%)
Na	-0.7783	0.5045	-0.0735
Mg	-0.7163	0.4540	-0.0097
P	0.6088	0.7082	0.0906
S	-0.2957	-0.8110	-0.2217
Cl	-0.6881	-0.4026	-0.1253
K	0.7849	-0.4115	0.0832
Ca	-0.3780	-0.2457	0.8900

Correlation between the variables and the main axes. The contribution of each axis to the total variation is indicated in brackets. 53 areas were measured on 6 different nuclei.

Cryoprocessed liver

Ultrastructure. As we have recently described (Quintana 1993, 1994), the ultrastructure was found to be satisfactory over 2 or 3 cell layers in the surface of cryofixed liver fragments (Fig. 7). Ice crystals were not observed in those nuclei located near the cryofixation front. Figure 8 shows examples of nuclei images obtained from unstained sections of about 1 μm. The contrast is weak but it is possible to identify the condensed chromatin, the nucleolus and the nucleoplasm (Figs. 8a and 8b). Local contrast enhancement of images allows a better display of these structures (Figs. 8c and 8d).

X-ray microanalysis. X-ray analysis of several cytoplasmic and nuclear areas is shown in Figure 9. Table 8 shows the results of wet mass fraction evaluation obtained from equation (5) in Appendix 1.

MSA of the X-ray spectra. The results from a set of 53 nuclear areas are shown in Table 9 and in Figure 10. We observe:

Figure 8 (on page 573). Rat hepatic tissues after cryoprocessing by cryofixation, freeze-substitution and cryoembedding. Nuclei from dry-cut sections of about 1 μm thick observed unstained in a 200 kV electron microscope. Bar = 2 μm. Digitalized electron images before (**a** and **b**) and after local filtering treatment (**c** and **d**).

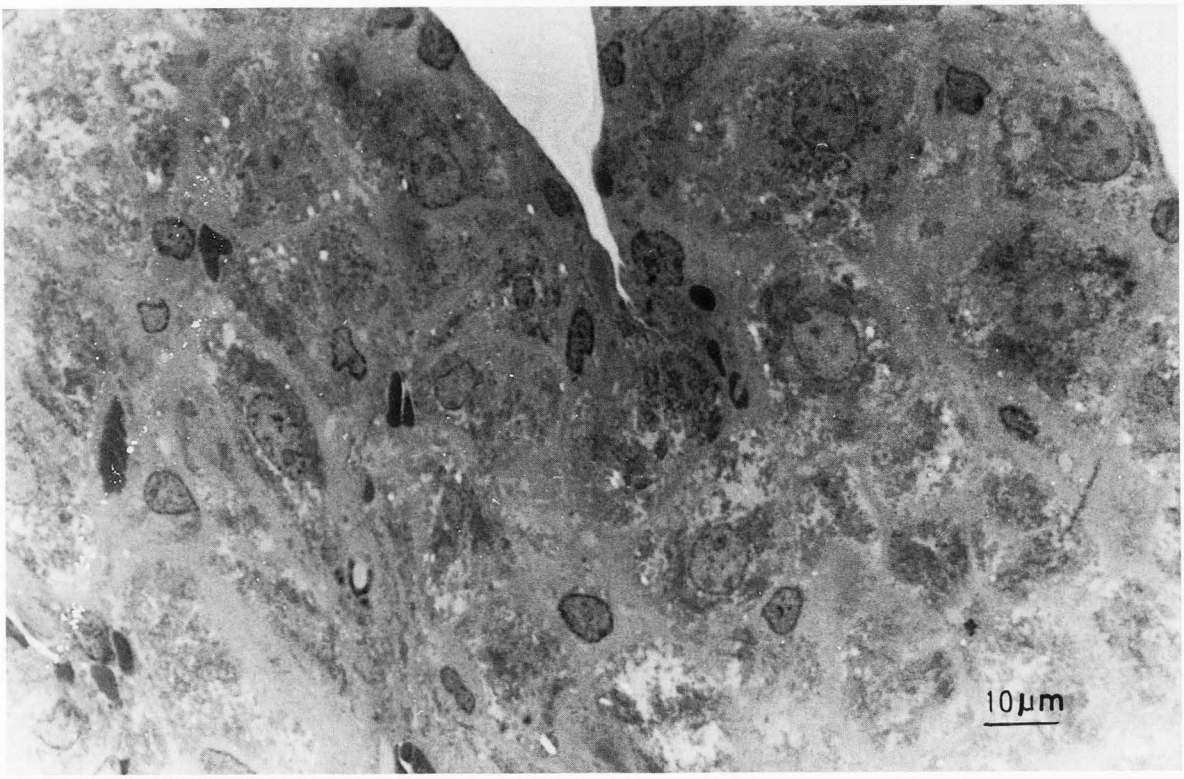

Figure 7. Morphology of rat hepatic tissues after cryoprocessing by cryofixation, freeze-substitution and cryoembedding.

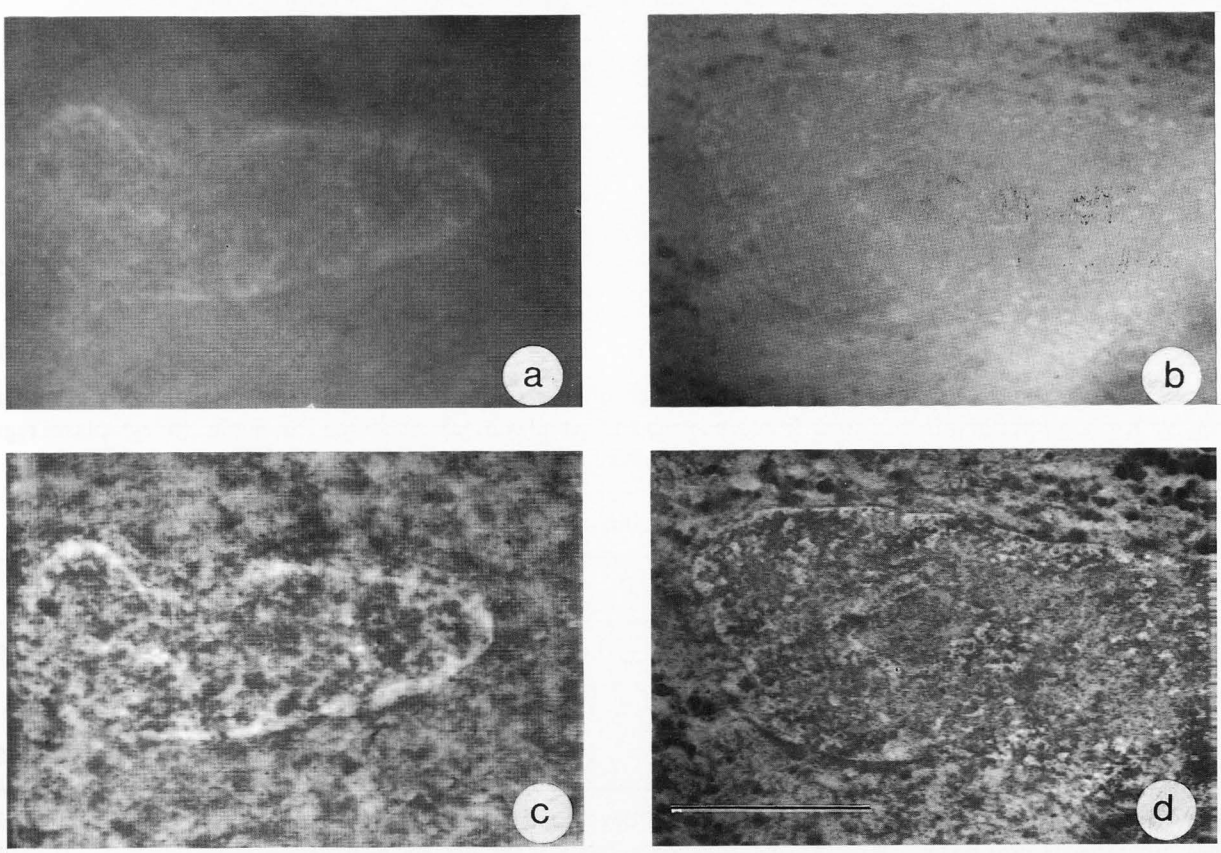

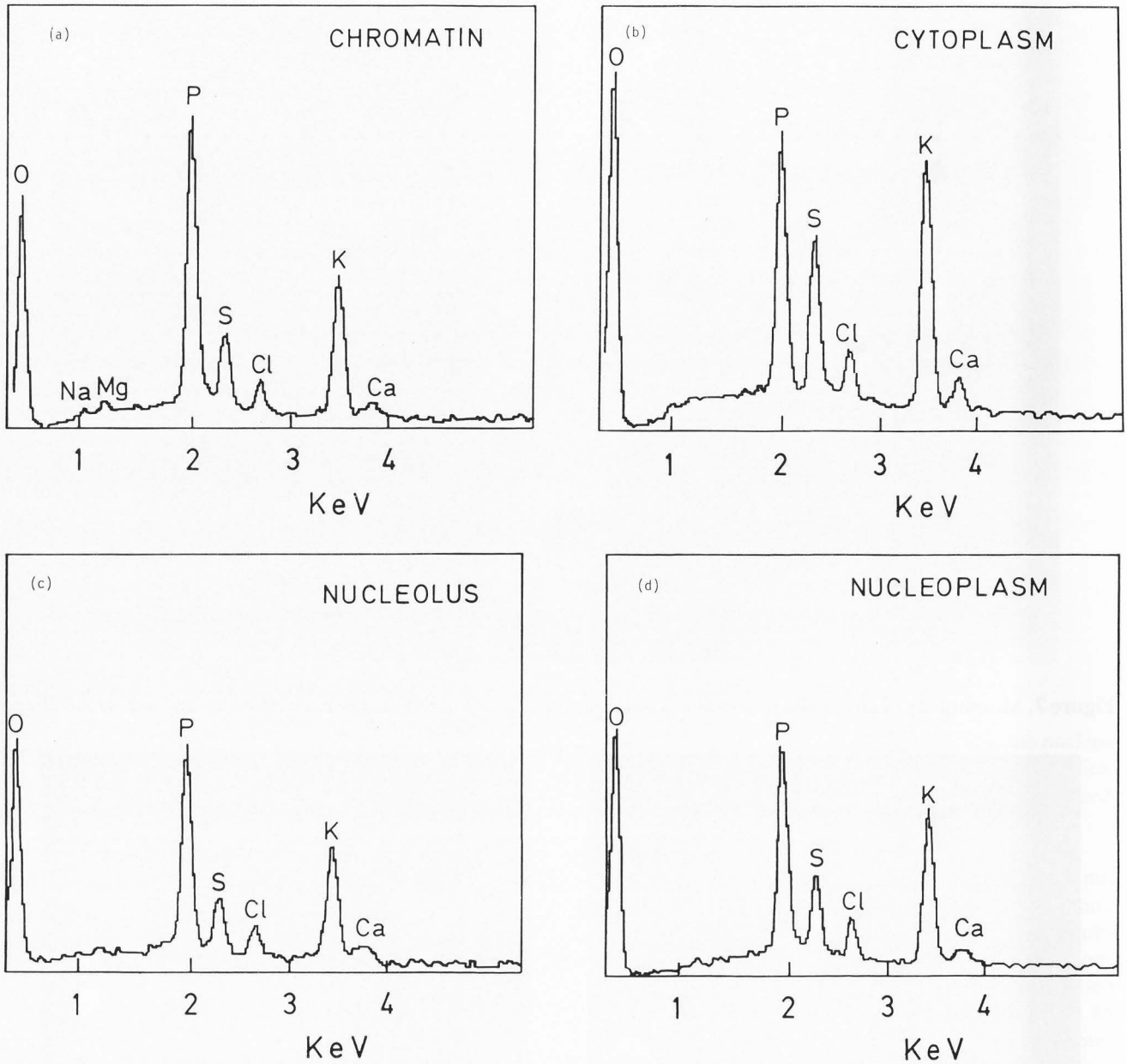

Figure 9. Rat hepatic tissues after cryoprocessing by cryofixation, freeze-substitution and cryoembedding. Energy dispersive X-ray spectra of different areas from a nucleus and cytoplasm, (a) condensed chromatin, (b) cytoplasm region next to the nucleus containing ribosomes, (c) and (d) nucleolus and nucleoplasm from a different cell.

Table 10. Mean values for the concentration in the groups.

	Na	Mg	P	S	Cl	K	Ca
G1 (n=24); N=4,5,6	6.8 ± 0.2	3.2 ± 0.1	49 ± 0.4	12.2 ± 0.3	7.3 ± 0.1	21.1 ± 0.2	0.6 ± 0.06
G2 (n=16); N=4,5,6	6.1 ± 0.6	3.0 ± 0.2	44 ± 1	16 ± 0.7	9.4 ± 0.4	21.2 ± 0.7	0.8 ± 0.1
G3 (n=13); N=1,2,3	2.1 ± 0.3	1.91 ± 0.2	48 ± 1	15 ± 0.8	5.8 ± 0.5	26.8 ± 0.6	0.5 ± 0.09

Concentration given as mean values ($*10^4$) (± standard deviation of the mean) in the three groups. n is the number of measurements of each group. N is the identification number of the nucleus analyzed.

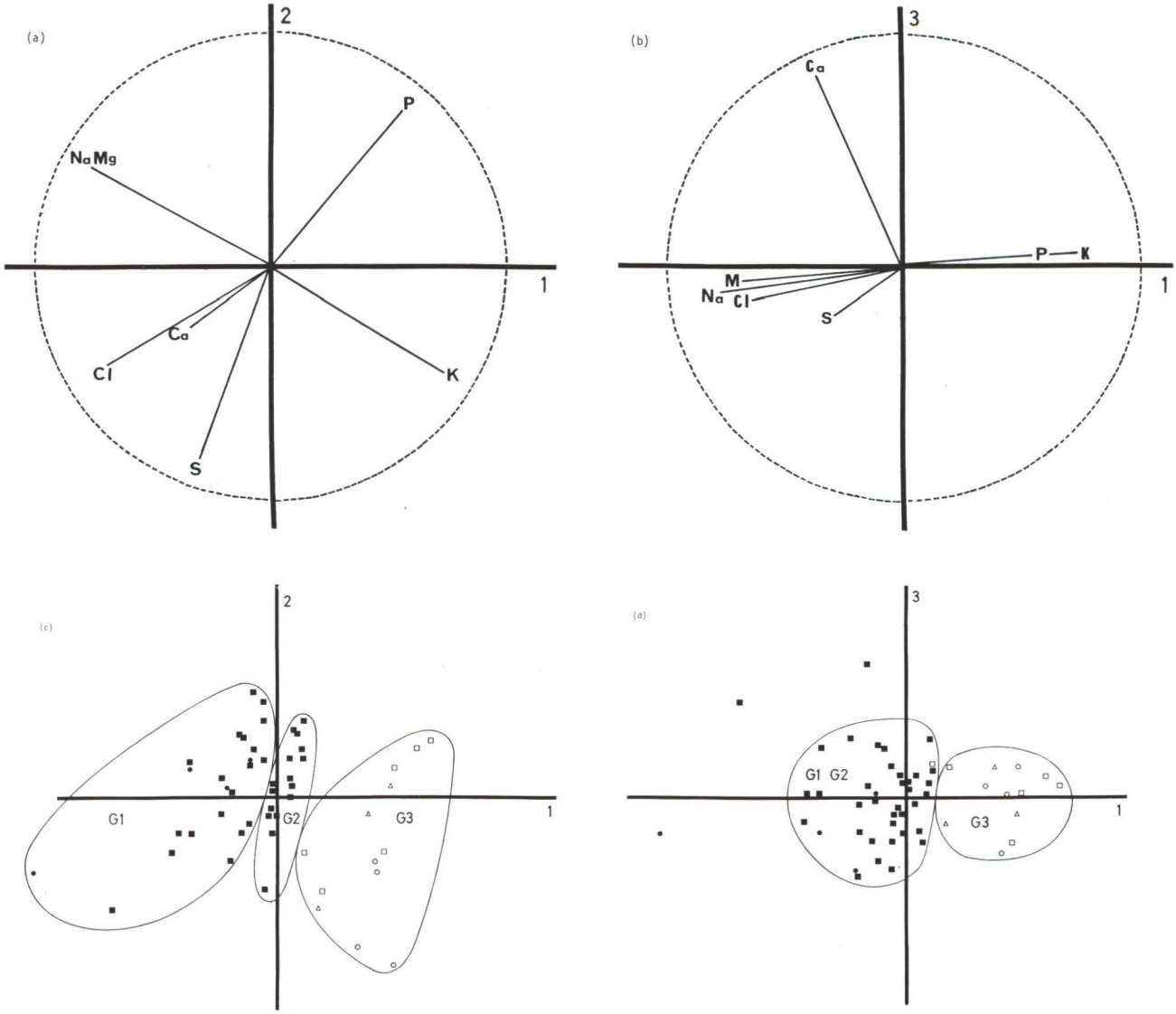

Figure 10. Rat hepatic tissues after cryoprocessing by cryofixation, freeze-substitution and cryoembedding. Results of PCA on a set of 53 areas from nuclei. Variable representation; (a) axes 1 and 2; (b) axes 1 and 3. Individuals representation ; (c) axes 1 and 2; (d) axes 1 and 3. (□) areas from nucleus N1; (△) areas from nucleus N2; (○) areas from nucleus N3; (●) areas from nucleus N4; (■) areas from nucleus N5.

---

(1) P and S are always anticorrelated (in the three axes);

(2) P is strongly correlated to K in axis 1. In axis 2, K is correlated to S and anticorrelated to P;

(3) Cl is always correlated to S; and

(4) Na and Mg are always correlated, and anti-correlated to K (in the three axes).

Axis 1 represents the opposition between the (P, K) elements group and the (Na, Mg, Cl, Ca et S) elements group. Axis 2 represents the opposition between the (P, Mg, Na) and the rest of elements (S, K, Cl and Ca).

The analyzed areas may be divided into three groups G1, G2, G3 in the factorial plane (1-2). Groups G1 and G2 consist of measurements over nuclei 4, 5 and 6 and group G3 is formed by measurements over nuclei 1, 2 and 3. The mean values for the concentrations in each group are shown in Table 10. The main difference between groups G1 and G3 is the concentration of certain elements such as Na and Mg (with a lower concentration in group 3) and K and S (with a higher concentration in group 3). There is no significant difference in the values of P between both groups. Groups G1 and G3 are formed by those areas which have been identified as condensed chromatin or nucleolus. The main difference between groups G1 and G2 is the concentration of elements such as S and Cl (higher in group 2) and P (lower

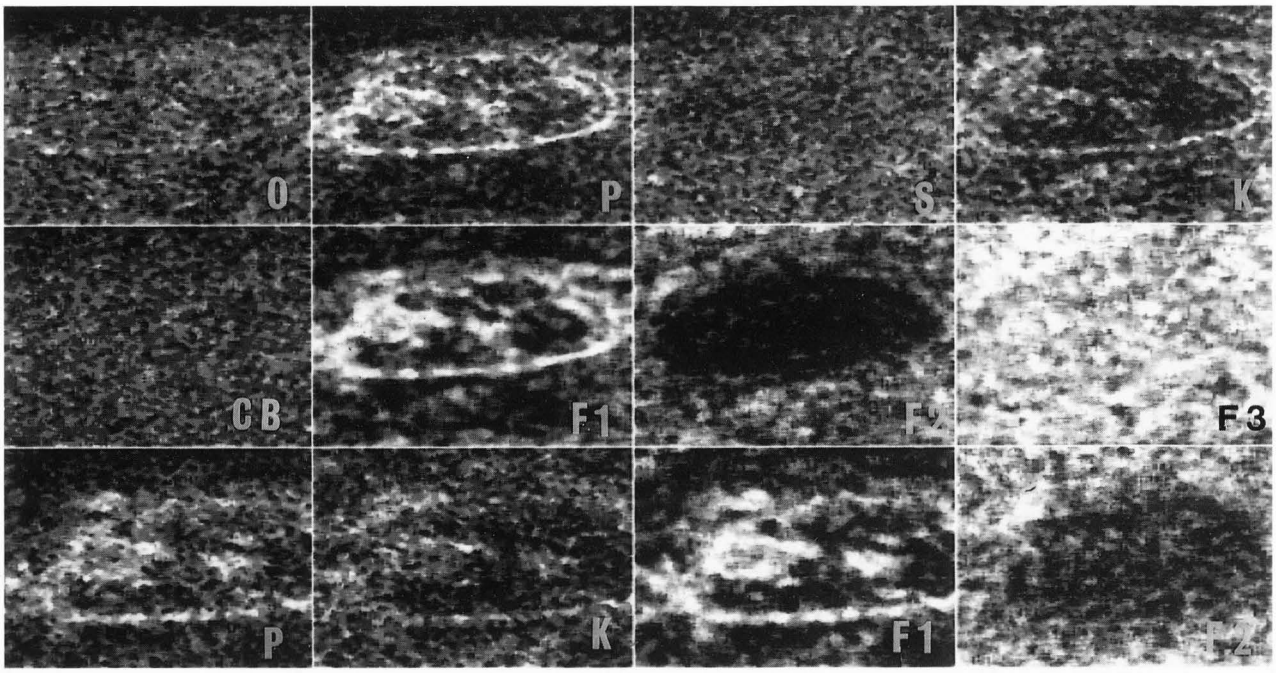

Figure 11. Rat hepatic tissues after cryoprocessing by cryofixation, freeze-substitution and cryoembedding. Elemental X-ray maps of O, P, S, K and continuum background X-ray image (CB) from one nucleus with the surrounding cytoplasm and factorial F1, F2 and F3 images. Bar = 5 μm. Last line shows P, K, F1, and F2 images of an area including the nucleolus that have been acquired with a stronger magnification. Bar = 2 μm.

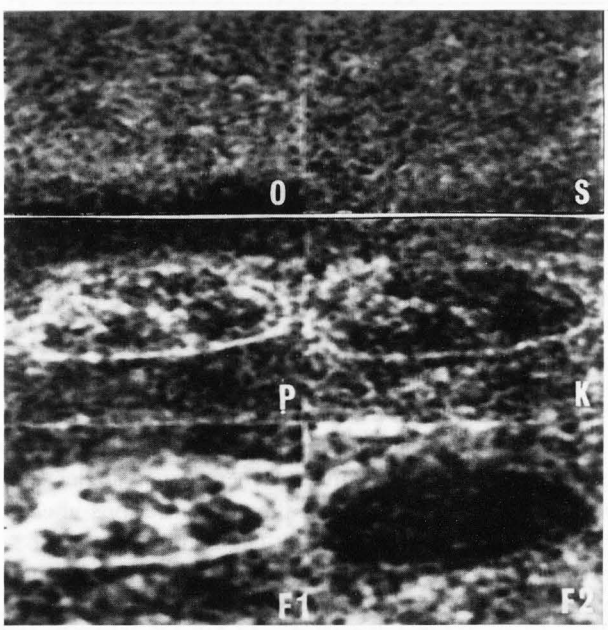

Figure 12. Enlarged images of O, P, S, K, F1 and F2 of the area shown in Fig. 11. The F1 images represent the stronger correlation between P and K in the nucleic acids (condensed chromatin and nucleolus). The F2 images represent the strong correlation between S and K in the cytoplasm (proteins).

in group 2). The concentration of K is the same in both groups. Group 2 is formed by those areas which have been identified as nucleoplasm and regions very close to the nuclear membrane which may include cytoplasm areas (remember that the sections are about 1 μm thick).

X-ray images. X-ray images for those elements with the highest concentration (O, P, K, and S) and for the X-ray continuum background image (CB) were registered (Figs. 11 and 12). The X-ray continuum image reveals mainly the mass-thickness effect (ρt) which has a very small variation among the different areas displayed in case of absence of heavy elements. Table 11 shows the number of counts obtained from the set of X-ray images displayed in Figure 11.

MSA of X-ray mapping. The FAC has been applied to series of 4 characteristic images from O, P, S and K (Tables 12 and 13). The results over areas including one nucleus with surrounding cytoplasm are shown in Figures 11 and 12. The nuclear areas which include the nucleolus were also recorded at larger magnification (Fig. 11).

The factorial images over axis 1 (F1) show how the P, K correlation separates those areas which mainly contain nucleic acids (chromatin and nucleolus) from the rest of the image. The factorial images over axis 2 (F2) show how the S, K correlation separates those areas

Table 11. Example of the number of total counts obtained from one set of images.

	oxygen	phosphorus	sulfur	potassium
average	30	9	8	8
stand dev	6	4	3	3
minimum	7	0	0	0
maximum	61	45	21	27

Table 12. Results from FAC

	Axis 1 (42.7%)	Axis 2 (30.7%)	Axis 3 (16.7%)
O	-0.0680	-0.0291	0.0315
P	0.2537	-0.1168	-0.0412
S	-0.0850	0.0822	-0.1727
K	0.1535	0.2301	0.0640

Variables analysis. Correlation between the variables and the main axes. The contribution from each axis to the total variance is shown in parentheses (16384 pixels analyzed). Set of images displayed in Figure 11.

Table 13. Results from FAC.

	Axis 1 (50%)	Axis 2 (30.4%)	Axis 3 (19.6%)
O	-0.0823	-0.0329	0.0377
P	0.2635	-0.1415	-0.0610
S	-0.0885	0.1267	0.2115
K	0.1973	0.2432	0.0985

Variables analysis. Correlation between the variables and the main axes. The contribution from each axis to the total variance is shown in parentheses (16384 pixels analyzed). Set of images displayed in Fig. 11 at a higher magnification.

---

which mainly contain proteins (cytoplasm and nucleoplasm) from the rest of image. The factorial images over axis 3 (F3) represent the statistical noise over the measurements of the element with the lowest concentration, S. Therefore, these images do not provide any more useful information.

Discussion

The relevance of *in situ* X-ray microanalysis in the form of static collected spectra or elemental maps, in obtaining physiopathological information on compartmentation of diffusible elements at subcellular levels is now well known. The subject has been recently discussed by LeFurgey *et al.* (1992). Although the interest in this research is strong, the complexity of the experiments and their high costs are also very important and few biology laboratories are equipped to perform such work. This is the case for the laboratories in France (Quintana and Nicaise, 1991). Therefore, we have carried out the experiments, observations and analyses in three different laboratories: two Physics-Biology Services, namely at Barcelona University (Spain) and Rouen University (France) and the Department for Metallurgic Research at CEA/Saclay (France). This is the reason why only a limited number of measurements and images have been taken.

Due to the small number of cells which have been analyzed, it is not our aim to give our results any definitive biological meaning. Our objective is to draw attention to the following facts.

Liver processed by the pyroantimonate method

In situ methods for the precipitation of free ions are sometimes criticized. This is the case for the method of precipitation by the pyroantimonate, for which a number of drawbacks have been mentioned:

(1) lack of specificity (PA can cause co-precipitation of several cations);

(2) imprecise localization (possible migration of precipitates on more or less important distances); and

(3) secondary nucleation phenomena (which affect the size of the precipitates).

For a detailed discussion of advantages and limits of this method see Mentré and Escaig (1988) and Mentré and Halpern (1988).

The experimental protocol was optimized by Mentré (1988) in order to obtain excellent localization of precipitates in Na^+ and Ca^{2+} rich zones of mouse skeletal muscle. We have therefore, used this improved experimental protocol. In the series of experiments we have analyzed, precipitates contain a higher concentration of K than in other experiments or with other experimental protocols. The high value for the K/P ratio within the precipitates (a mean of 1.7) seems to indicate that K is mainly provided by the reagent, potassium pyroantimonate. In fact, the possibility of the coprecipitation of K with other cations in the antimonate salts has been pointed out by Simson and Spicer (1975).

Larger quantities of calcium are also found in nuclear regions without precipitates and identified as chromatin and nucleolus. The Ca/P ratio measurements (a mean of 3.3×10^{-1}) and the Ca/S ratio measurements (a mean of 1.1) show that these calcium concentrations are

much higher than the physiological values (Ca/P about 7.5×10^{-3}: Ca/S about 1.8×10^{-2}). This is also the case in conventional chemical prepared samples and in chemically fixed, PLT dehydrated and low temperature (HM20 or K11M Lowicryl) embedded quail oviduct cells, and rat follicular and oocyte cells (Quintana and Ollacarizqueta, 1989; Quintana, 1991).

Despite these "artefacts" (high concentration of K in precipitates and high concentration of Ca in condensed chromatin and nucleolus), and since all the precipitates contain Na (in variable quantity), Mg and often Ca, we thought that the analysis of X-ray spectra and X-ray maps obtained on different zones by MSA could bring new information concerning the distribution of the precipitable part of cations (Na^+, Mg^{2+} and Ca^{2+}) in the nuclei. In fact, as Mentré (1989) pointed out for the hepatocyte nuclei, the precipitable cations are mainly found in the nucleoplasm. This is also the only nuclear compartment that always contain precipitates in rat parotid (Simson and Spicer, 1975) independently of the variant of the potassium pyroantimonate technique used.

The high variety of "patterns" formed by the precipitates in nucleoplasm would show that the observed nuclei are in different physiological states. The presence of precipitable cations Na^+, Mg^{2+} and Ca^{2+} is also observed within certain fibrillar centers of the nucleolus. Some of these patterns look like the argyrophilic proteins distribution (Ploton *et al.*, 1987; Robert-Fortel *et al.*, 1993). Perhaps the Ag has replaced one of these cations which are weakly bound to the proteins.

The results obtained by MSA are:

(1) despite the presence of K, MSA applied to series of spectra allowed two sub-populations of precipitates in the nucleoplasm to be differentiated, with the Na concentration as discriminant factor;

(2) the high affinity of Ca with chromatin and nucleolus is confirmed in the MSA results by the high correlation between Ca, P and S;

(3) the opposition between intranuclear regions (with or without precipitates) can be visualized by the anti-correlation between the two groups of variables (Sb, K, Na) and (P, S). The two compartments can be easily observed within the factorial images F1 and F2 obtained from series of four elemental maps (Sb or K, P, S, O). We conclude that, despite the limitations described above, the technique of precipitation by pyroantimonate can be used (in association with X-ray microanalysis and MSA) in order to get information concerning the distribution of free or weakly bound cations Na, Mg and Ca at the subcellular level, in different metabolic states. A more complete study with a larger number of samples is, however, necessary before a definitive conclusion can be reached.

The usefulness of MSA methods in the exploitation of microanalytic data obtained on cryoprocessed samples

MSA methods allow a better interpretation of the results than other statistical methods. They allow a graphical display of the correlations between the elements analyzed and the separation of the cellular compartments depending on their composition.

In spite of the limited number of measurements we have been able to confirm the results obtained by other authors, especially the following ones:

(1) The P, K correlation separates areas rich in nucleic acids (condensed chromatin and nucleolus) from the nucleoplasm and the cytoplasm. The potassium would then be bound to the phosphate groups of nucleic acids (Cameron *et al.*, 1990; Warley, 1992).

(2) Some of the analyzed nuclei show a high concentration of Na and Mg in parallel with a low concentration of K. This would support the exchange possibilities between K and Na (and Mg ?) and would show different "natural" metabolic nuclear states (see Negendank, 1989; Cameron *et al.*, 1990). This would also be the case for the excised rat liver cells (Zierold, 1988; Quintana, 1991), in which the exchange between K and Na is much higher due to the metabolic perturbations provoked during the sampling process. An extreme case would be the total replacement of K (and Na) by Ca in conventional electron microscope preparations (chemical fixation and alcohol dehydration).

(3) The S, K correlation separates the proteins from the nucleic acids. K would be bound to the HCO_3^- and/or SO_4^{2-} groups in proteins (Cameron *et al.*, 1990; Edelmann, 1980).

(4) Cl is always correlated to S (proteins). The suggested cation to be bound to Cl^- would be the NH_3^+ group from proteins (Cameron *et al.*, 1990).

(5) The interpretation of the results from Ca is not easy due to the low concentrations of this element and the measurement problems arising when there are high K concentrations. In our preparations, only the images for those elements with a high concentration C, O, P, S and K have been displayed. Carbon images are homogeneous. The oxygen within the cryoprocessed cells has a higher concentration in the condensed chromatin. The P, K and S maps have a low signal-to-noise ratio. The maximum dwell time is limited in the TEM/STEM (Philips CM20) used to about one hour (due to the stability of the cold stage). In our conditions the maximum of potassium counts in hepatic cells (192 counts/sec) may be compared to that obtained by LeFurgey *et al.* (1992), (499 counts/sec) in kidney cells. The ratio (2.6) between these two values is approximately that of the ratio for the dry and wet weight concentrations. It should be stressed that similar qualitative results con-

cerning the correlation and anticorrelation between elements were obtained by static probe spectroscopy and by elemental mapping.

The factorial images of P, K correlation would be very useful for displaying cells in different physiopathological stages. One example would be the apoptotic cells in the thymus gland for which the correlation between P and K in chromatin is lost (Warley, 1992).

Conclusion

Digital X-ray elemental mapping has proved to be a very powerful tool to deal with problems in cell physiology (Somlyo, 1984; LeFurgey *et al.*, 1988; Johnson *et al.*, 1988; Saubermann and Heyman, 1987; LeFurgey *et al.*, 1992). Results obtained from mapping are not as accurate as those obtained from static probes over long periods of time. However, mapping provides data from a much larger number of areas, thus meaningful biological trends would be collected in about the same time as it would take to collect data from a few static probes.

There are several ways to increase the level of statistical significance of mapping:

(1) **Increased dwell time**. This is limited by the stability of the instrument and of the sections.

(2) **Simultaneous acquisition of X-ray and electron energy loss spectroscopy (EELS) images**. The simultaneous acquisition of X-ray images for O, P, S and K and EELS images for O, N, Cl, Na, Mg and Ca would be possible if an analytical electron microscope (AEM) with X-ray ultra-thin window (UTW) and parallel EELS acquisition (PEELS) spectrometers were available. In fact, it has been proven that EELS spectrometry has a better sensitivity than X-ray spectrometry for the latter elements (Leapman and Hunt, 1991).

(3) **Use of MSA**. MSA would then allow the global treatment of the information provided simultaneously by the X-ray and EELS images on relatively low-statistical elemental maps.

(4) **Use of static probes in association with MSA**. Areas which are considered the most interesting may be analyzed by means of static probes over longer periods of time. When analysis is performed with two-dimensional incremental position of the probe, it is possible to display the results of MSA spectra processing as a low-resolution image. This can help to interpret these results by incorporating the spatial information (De Bruijn *et al.*, 1987).

Thus, the task of displaying objective results concerning correlation (and anticorrelation) between the diffusible and non-diffusible elements in cell compartments would be much easier.

Acknowledgements

The authors wish to thank Dr. Duval and Dr. Lemarchand from the Electron Microscope Service of Rouen University (France) for the technical support and Dr. Boulanger from C.E. Saclay/DTA/CEREM/SRMP (France) for giving us access to AEM Philips CM20 and for helpful discussions. We would also like to thank Dr. P. Mentré for her assistance in the preparation of pyroantimonate treated samples. This work was partially supported by the Mercure French Spanish Program (Barcelona University, Spain)

References

Benzecri JP (1978) L'analyse des Données (Analysis of Data). Dunod, Paris.

Bonnet N, Simova E, Thomas X (1991) Application of multivariate statistical analysis to time dependent spectroscopy. Microsc Microanal Microstruct **2**: 129-142.

Bonnet N, Trebbia P (1992). Multi-dimensional data analysis and processing in electron-induced microanalysis. Scanning Microsc Suppl **6**: 163-177.

Cameron IL, Hardman WE, Hunter KE, Haskin C, Smith NKR, Fullerton GD (1990) Evidence that a major portion of cellular potassium is "bound". Scanning Microsc **4**: 89-102.

Cliff G, Lorimer GW (1975) The quantitative analysis of thin specimens. J Microsc **103**: 203-207.

De Bruijn WC, Koerten HK, Cleton-Soeteman MI, Blok-van Hoek CJG (1987) Image analysis and X-ray microanalysis in cytochemistry. Scanning Microsc **4**: 1651-1667.

Edelmann L (1980. Potassium binding sites in muscle. Electron microscopic visualization of K, Rb, and Cs in freeze-dried preparations and autoradiography at liquid nitrogen temperature using ^{86}Rb and ^{134}Cs. Histochemistry **67**: 233-242.

Foucard T (1982) Analyse Factorielle: Programation sur Microordinateur (Factorial Analysis: programming on a Microcomputer). Masson, Paris.

Gupta BL (1989) 1 μm thick frozen hydrated/dried sections for analyzing pericellular environment in transport epithelia; new results from old data. In: Electron Probe Microanalysis. Applications in Biology and Medicine (Zierold K, Hagler HK, eds.), Springer-Verlag, Berlin, pp 199-211.

Hall TA (1991). Suggestions for the quantitative X-ray microanalysis of thin sections of frozen-dried and embedded biological tissues. J Microsc **164**: 67-79.

Halpern S, Quintana C (1989) Two simple devices for cryofixation and cryoembedding. Biol Cell 67:10a (abstract).

Hannequin P, Bonnet N (1988) Application of multivariate statistical analysis to energetic image series. Optik **81**: 6-11.

Johnson DE, Izutsu K, Cantino M, Wong J (1988) High spatial resolution spectroscopy in the elemental microanalysis and imaging of biological systems. Ultramicroscopy **24**: 221-236.

King P, Browning R, Pianetta P, Lindau I, Keenlyside M, Knapp G (1989) Image processing of multispectra X-ray photoelectron spectroscopy images. J. Vac Sci Technol **7**: 3301-3304.

Komnick H (1962) Elektronenmikroskopische Lokalisation von Na^+ und Cl^- in Zellen und Geweben (Electron microscopical localization of Na^+ and Cl^- in cells and tissues). Protoplasma **55**: 231-244.

Leapman RS, Hunt JA (1991) Comparison of detection limits for EELS and EDXS. Microsc Microanal Microstruct **2**: 231-244.

Lebart L, Morineau A, Fenelon JP (1979) Traitement des Données Statistiques: Méthodes et Programmes (Treatment of Statistical Data: Methods and Programs), Dunod, Paris.

LeFurgey A, Bond M, Ingram P (1988) Frontiers in electron probe X-ray microanalyis: application to cell physiology. Ultramicroscopy **24**: 185-220.

LeFurgey A, Davilla SD, Kopf DA, Sommer JR, Ingram P (1992) Real-time quantitative elemental analysis and mapping: microchemical imaging in cell physiology. J Microsc **165**: 191-223.

Mentré P, Escaig F (1988) Localization by pyroantimonate. I. Influence of the fixation on the distribution of calcium and sodium. An approach by analytical ion microscopy. J Histochem Cytochem **36**: 48-54.

Mentré P, Halpern S (1988) Localization by pyroantimonate. II. Electron probe microanalysis of calcium and sodium in skeletal muscle of mouse. J Histochem Cytochem **36**: 55-64.

Mentré P (1989) Application of the pyroantimomate method and electron probe microanalysis to the study of glycogen metabolism in liver. Scanning Microsc **3**: 495-504.

Negendank W (1989) The physical state of potassium in the human lymphocyte: a review. Scanning Microsc **3**: 865-875.

Paque J, Browning R, King P, Pianetta P (1990) Quantitative information from X-ray images of geological materials. In: Microbeam Analysis 1990, San Francisco Press, San Francisco, pp 195-198.

Ploton D, Beorchia A, Menager M, Jeannesson P, Adnet JJ (1987) The three-dimensional ultrastructure of interphasic and metaphasic nucleolar argyrophilic component studied with high voltage electron microscopy in thick sections. Biol Cell **59**: 113-120.

Quintana C, Ollacarizqueta A (1989) Multivariate statistical analysis of electron probe microanalytical data on cell nuclear constituents. Ultramicroscopy **28**: 315-319.

Quintana C (1991) X-ray microanalysis of cell nuclei. J Electron Microsc Techn **18**: 411-423.

Quintana C, Nicaise G (1991). Biological applications of electron probe microanalysis in France. J Electron Microsc Techn **18**: 424-428.

Quintana C (1992) Development of a new cryosystem of freeze-substitution and cryoembedding for processing biological samples. In: Electron Microscopy 1992, Vol 1 (Rios A, Arias JM, Megías-Megías L, eds), Proc EUREM 1992, Universidad de Granada, Granada (Spain), pp 363-364.

Quintana C (1993) *In situ* conservation of diffusible elements in liver cells after cryofixation, cryosubstitution and low temperature embedding at 193 K in HM23 Lowicryl resin. Microsc Research Techn **24**: 103-104.

Quintana C (1994) Cryofixation, cryosubstitution and cryoembedding for ultrastructural, immunocytochemical and microanalytical applications. Micron **25**: 63-99.

Robert-Fortel I, Junera HR, Geraud G, Hernandez-Verdun D (1993) Three-dimensional organization of the ribosomal genes and Ag-NOR proteins during interphase and mitosis in PtK1 cells studied by confocal microscopy. Chromosoma **120**: 146-157.

Saubermann AJ, Heyman RV (1987) Quantitative digital X-ray imaging using frozen hydrated and freeze-dried tissues sections. J Microsc **146**: 169-182.

Simson JAV, Spicer SS (1975) Selective subcellular localization of cations with variants of the potassium (pyro)antimonate technique. J Histochem Cytochem **23**: 575-598.

Somlyo AP (1984) Compositional mapping in biology: X-ray and electrons. J Ultrastruct Res **88**: 135-142.

Somlyo AP, Bond M, Somlyo AV (1985. Calcium content of mitochondria and endoplasmic reticulum in liver frozen rapidly in vivo. Nature **314**: 622-625.

Trebbia P, Bonnet N (1990) EELS elemental mapping with unconventional methods. I. Theoretical basis: image with multivariate statistics and entropy concepts. Ultramicroscopy **34**: 165-178.

Trebbia P, Mory C (1990) EELS elemental mapping with unconventional methods. II. Applications to biological specimens. Ultramicroscopy **34**: 179:203.

Von Zglinicki T, Bimmler M (1987). The intracellular distribution of ions and water in rat liver and heart muscle. J Microsc **146**: 77-85.

Warley A (1992) Studies on lymphocytes and thymocytes using X-ray microanalysis. In: Electron Microscopy 1992, Vol 3 (Rios A, Arias JM, Megías--Megías L, eds) Proc EUREM 1992, Universidad de Granada (Spain): pp 559-560.

Zierold K (1988). X-ray microanalysis of freeze-dried and frozen-hydrated cryosections. J Electron Microsc Techn **9**: 65-82.

Appendix 1. The Cliff-Lorimer Method Applied to Biological Specimens

The Cliff-Lorimer method which is widely applied in material science can be used to determine concentrations of elements in biological specimens. If C_x and C_y are the weight fractions of two chemical elements x and y present in a thin film, and S_x and S_y the corresponding characteristic X-ray signals, then a relative quantitative analysis may be obtained by:

$$C_x/C_y = K_{xy} (S_x/S_y) \quad (1)$$

In this relation K_{xy} is the Cliff-Lorimer constant, which can be calculated by the expression:

$$K_{xy} = [D_x (Q\omega\xi/A)_x)]/[D_y(Q\omega\xi/A)_y] \quad (2)$$

where Q is the ionization cross-section for K, L or M lines, ω is the fluorescence yield for these lines, ξ is the relative intensity factor of the measured line, A is the atomic weight and D is the EDS detector efficiency. The K_{xy} constant may be also measured by using the appropriate standard samples containing known concentrations of x and y.

If the sample does not comply with the thin film criterion (no significant absorption in the sample) this effect should be corrected. The absorption correction factor (ACF) is

$$ACF = \frac{(\mu/\rho)_x [1 - \exp(-\mu/\rho)_y \rho t \,.\, \csc \alpha]}{(\mu/\rho)_y \{1 - \exp(-\mu/\rho)_x \rho t \,.\, \csc \alpha]} \quad (3)$$

where $(\mu/\rho)_x$ and $(\mu/\rho)_y$ are the mass absorption coefficients for the characteristic radiation of x and y, respectively, ρ is density, t is thickness, and α is the angle between the detector axis and the specimen surface.

This correction is necessary for one μm-thick specimens containing the pyroantimonate but is negligible for cryoprepared specimens. Examples are given in Table 14.

This relative quantification method becomes an absolutely quantitative method when all the chemical elements, j, present in the sample, can be analyzed. In this case one may state that $\Sigma C_j = 1$ and thus we have a number of independent relations equal to the number of chemical elements in the sample.

With the UTW X-ray detectors all elements of a biological sample can be measured except for hydrogen. From a theoretical point of view it would be possible to

Table 14. Absorption correction in different types of specimen.

	zones with high Sb concentrations	zones without Sb	cryosections
Na	2.135	1.314	1.074
Mg	1.875	1.201	1.049
P	0.811	0.950	0.987
S	0.762	0.950	1.033
Cl			1.025
K	0.580	0.894	1.000
Ca	0.568	0.892	1.000
Sb	0.553	0.883	
density (g/cm^3)	6	1.3	1

Section thickness in all cases 1000 nm.

---

apply the Cliff-Lorimer method by using the relation:

$$\Sigma(Cj\text{-}[H]) = \text{Constant} \quad (4)$$

as the n^{th} relation because the [H] concentration in the different cellular compartments may be considered constant with an approximate value of 6%.

In practical work this is uncertain because:

(1) the EDS detector efficiency and the mass absorption coefficients for carbon, nitrogen and oxygen are not well known; and

(2) carbon and oxygen may be partially lost under the extremely high electron dose required for the X-ray analysis (unpublished results).

Moreover, the Cliff-Lorimer method can be used for evaluation of the mass-fraction of other elements than C, N and O. In fact the quantitative measurements performed with the Hall method by several authors show that the addition of wet mass fractions of the elements Na, Mg, P, S, Cl, K and Ca varies between 0.0077 and 0.0178 in the different cellular compartments (von Zglinicki and Bimmler, 1987; Zierold, 1988; Gupta, 1989).

$$\text{If } \Sigma(\text{Na, Mg, P, S, Cl, K and Ca}) = 0.01 \quad (5)$$

is used as the n^{th} relation then an evaluation of the wet mass fractions of these elements may be obtained from Lowicryl embedded samples.

Relation (5) cannot be applied to samples treated by the pyroantimonate method. Instead, we have used equation (6):

$$\Sigma(\text{Na, Mg, P, S, Cl, K, Sb, Ca}) = \text{constant} = 100 \quad (6)$$

Table 15. Ratio between calculated peaks and standard spectrum peaks (K-ratio).

Lines	Intensity (cts/sec)	2 sigma error	K-ratio
P Kα	79.28	0.0106	1.0422
S Kα	28.17	0.0284	1.0694
Cl Kα	30.49	0.0268	0.9383
Bi Mα	86.50	0.0205	1.0114

Chi-squared: 5.4327

---

so that the MSA analysis can be applied to data obtained in different microscopes.

Appendix 2. Deconvolution of Overlapping Peaks

The Gaussian/Deconvolution program of the Quantum Kevex 8000 analyzer computer has been tested on the overlap of SKα peak (E = 2.307 keV), BiMα peak (E = 2.416 keV) and ClKα peak (E = 2.621 keV), as follows.

First, we added up, channel by channel, two standard spectra: (1) the spectrum of purified Bi and (2) the spectrum of a cell nucleus containing P, S and Cl (Fig. 13). Second, the resulting spectrum was treated following identification of P, S, Bi and Cl elements by using the Gaussian/Deconvolution program which calculates the characteristic peaks of P, S, Bi and Cl. The deconvolution "quality factor" is the ratio (K) between the calculated peaks and the standard spectrum peaks. The K-ratios are shown in Table 15 and are very close to unity which shows the reliability of the program.

Discussion with Reviewers

U. Lindh: It must be very hard to accurately assess the calcium concentration in the precipitates with interferences both from potassium and the high antimony concentration. How accurate is the assessment?

Authors: Yes, you are correct. One of the programs used for deconvolution (the Kevex 8000 Microanalyst) had been previously tested (see Appendix 2). For some precipitates, the results of the program was a zero concentration for Ca. This is the reason that we stated: "the Ca concentration in certain intranuclear precipitates is lower than the minimum concentration which may be detected in our experimental conditions".

U. Lindh: How do you interpret the fact that carbon is uniformly distributed whereas the density varies in the sections? Is there no carbon at all present in the precipitates?

Authors: The carbon is always present in the spectra of one PA precipitate or groups of PA precipitates. However, this does not prove that the precipitates contain carbon, because in any case, we analyze the surrounding organic matrix (which contains carbon) at the same time as the precipitates. The X-ray maps of liver tissues treated with the PA method were acquired, at different dates, in two different microscopes. In the first series of maps, we essentially acquired maps of C, O, Sb and P elements and eventually N and K maps, and we did not acquire the X-ray continuum maps. These maps had a very low S/N ratio (the TEM/STEM was equipped with a conventional tungsten gun, see Table 1). Nevertheless, in this series, we observed the correlation between the regions rich in Sb and the regions rich in K and probably also the anticorrelation between the regions rich in P and the regions rich in Sb (or K). The O maps, non-uniformly distributed, were difficult to interpret and the C maps were practically homogeneous and also non-interpretable.

In the second series of images we have not recorded the carbon maps. Therefore, we cannot give an answer to your question about the distribution of C in liver prepared by the PA method.

However, for cryoprepared specimens (cryoembedding in Lowicryl), we can ascertain that the concentration of C does not vary significantly for different specimen areas (see Table 16).

U. Lindh: Have you accounted for possible deviations from the Gaussian distribution when your samples sizes were very low?

Authors: We do not assume a Gaussian distribution and therefore we did not try to account for possible deviation. We did not attempt to draw statistical conclusions from this preliminary work.

U. Lindh: What are your expectations of the development of multivariate statistical methods in elemental analysis?

Authors: As we tried to explain throughout this paper, MSA is not a "magic trick" which could replace the hard experimental work necessary for the obtention of microanalytical data. It is only a practical tool for analyzing the content of the resulting experimental data set. Compared to more common methods for evaluating this content, it has the following characteristics:

(1) the whole data set is considered at once, instead of comparing elements (or biological compartments) pairwise;

(2) it is rather objective (no strong *a priori* hypotheses have to be made); and

(3) the results can be displayed graphically, which helps in the interpretation.

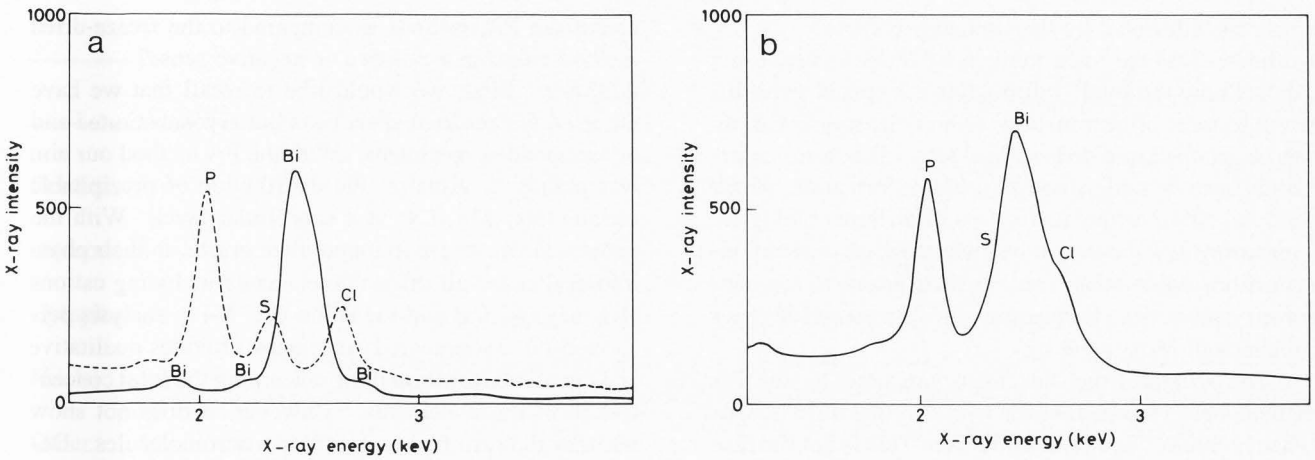

Figure 13. Spectra used for testing the Gaussian/Deconvolution program of the Quantum Kevex 8000 analyzer system: (a) Standard spectra of purified bismuth (solid line) and of a cell nucleus (dotted line) containing P, S and Cl. (b) Spectrum resulting from the addition, channel by channel, of the two standard spectra. The resulting spectrum is treated by using the Gaussian/Deconvolution program. The K-ratios are shown in Table 15.

Table 16. Composition of biological material (mass fraction).

	H	C	N	O	Sum
hydrated material	9.91	15.19	2.82	70.76	98.68
Dehydrated biological material[1]	7.36	50.42	9.76	28.37	95.91
Protein	7	50	16	25	98
DNA	4.2	38	16.7	31.2	90.1
Lipids[2]	12	77	0.8	9	98.8
Epon	8.4	61.1	0.3	25.3	95.1
Lowicryl HM20[2]	9.3	66.6	0.0	24.1	100
HM20 embedded material[3]	8.72	61.75	2.93	25.38	98.78

[1]From Boekestein *et al.* (1983) Scanning Electron Microsc **1983**; II, 725-736.

[2]From Reichelt and Engel (1989) Scanning Microsc **3**: 43-55.

[3]computed by assuming that the average concentration of water is 70%.

Though some drawbacks of the method must be expected (they still have to be investigated), we think that it will be useful for most of the applications of microanalysis which concern several elements and/or several specimen compartments. We think that the visual nature of elements maps does not protect the microanalyst from subjectivity and that an objective way to evaluate the maps is essentially useful. More specifically, one can expect that this kind of analysis will provide a way to go from chemical maps (distributions of e.g., P, S, O, or K) to molecular maps (distributions of nucleic acids, proteins).

W.C. de Bruijn: A large number of spectra, obviously collected at various dates and from different instruments under different conditions are objectively processed by the described methods to extract the requested correlation between the karyoplasmatic or cytoplasmic elements. However, the spectral processing to come to the conclusions about the absence/presence of the elements selected is not critically described. Would it not be advisable to include, in the set of correlation exercises, steps that demonstrate that the sampling of the spectra from the various sources did not influence the final conclusions, or to indicate to the reader that such sampling

errors are alleviated by the applied processes?

Authors: It is the main purpose of MSA to detect in a data set how the total "information" is spread over different sources of information, or how the measurements can be grouped into different subsets. The term "information" can be understood as useful information, which concerns either different elements or different biological compartments. It can also be understood as unuseful information, when some experimental artefacts are concerned [see e.g., Hannequin and Bonnet (1989) or Trebbia and Mory (1990)].

The spectra from specimens prepared by the PA method were recorded within two different microscopes (Hitachi 800MT and JEM 2000FX). This is not the case for the spectra from cryoprepared tissues which were only recorded with the JEM 2000FX. If the spectra recorded with different microscopes had given different results, this would lead to "the microscope" as being a specific "source of information". This means that measurements performed with a given microscope would be displayed close together. The fact that measurements are grouped according to the biological compartments rather than according to the microscope from which they originate (especially on factorial axis 1) means that the "microscope" information is of second order compared to the "compartment" information.

W.C. de Bruijn: Similarly, the images are acquired in a different instrument under quite different instrumental conditions. Would the authors please indicate, in the present application of the correlation technique, that these instrumental differences can be ignored.

Authors: It is true that X-ray maps of specimens prepared by the PA method were acquired within two different TEM/STEM instruments (Hitachi 800MT and Philips CM20). This is not the case for cryoprepared tissues which were only observed with the CM20 microscope. Anyway, series of elemental maps were not mixed when submitted to MSA: an analysis concerns only one series of different element maps recorded for a given specimen area at a given magnification. Its aim is to condense and describe the total information contained in the whole series into a reduced set of qualitative facts concerning either elements (e.g., element X is highly correlated with element Y on factorial axis 1) or biological compartments (e.g., compartment A behaves like compartment B on factorial axis 1). The key point of our analysis is that the same qualitative results (in terms of correlation or anti-correlation between elements) were obtained regardless of the microscope used.

W.C. de Bruijn: In the **Introduction** one of the aims was to correlate also the results of the two tissue preservation techniques. Would the authors comment on the use of the PA methods as compared to the freeze-dried method either in a positive or negative sense?

Authors: First, we would like to recall that we have not used freeze-dried specimens but cryosubstituted and cryoembedded specimens. With the PA method our aim was mainly to visualize the distribution of precipitable cations (Na, Mg, Ca) at a subcellular level. With the cryomethods, we try to immobilize *in situ*, in their physiological state, **all** diffusible elements including cations (Na, Mg, K, Ca) and the anion Cl. X-ray analysis performed on cryoprepared specimens provides qualitative and quantitative information concerning the **total** concentration of these elements. However, it does not show whether they are free or bound to macromolecules. Despite the limitations of the precipitation method, it seems that the two methods can help to obtain complementary information.

T. von Zglinicki: The simplest explanation for all results from the potassium pyroantimonate (PPA)-treated livers is that the precipitation reaction failed in the hand of the authors. K is still the major ion colocalized with Sb. That means that most of the precipitate is simply PPA-"fallout" without any histochemical reaction. The localization of the PPA crystals in the decondensed chromatin is probably due to heterogeneous nucleation, see Jong *et al.* (1982) Histochem J, **14** and von Zglinicki and Punck (1986) Histochem J, **29**.

Authors: We have used the PPA method modified by Mentré for localization of Na and Ca (and Mg). This modified method does not use osmium tetroxide in the fixative because osmium tetroxide causes loss of sodium [Van Iren *et al.* (1979) Histochemistry **63**: 273]. The experimental protocols were optimized to get an excellent localization of precipitates in Na^+ and Ca^{2+} rich zones of mouse skeletal muscle.

The possibility of the coprecipitation of K with other cations in the antimonate salts has been pointed out by Simson and Spicer (1975): "Precipitation could occur by replacement of any single dissociable cation by another less dissociable one, with retention of part or all of the K".

As Mentré pointed out, several sources of participating cation can be assumed: (1) free cations distributed according to diffusion, (2) loosely bound cations which were freed from their sequestration sites by the fixative procedures, and (3) tightly bound ions in macromolecules, unable to bind PA, but that can be detected by X-ray microanalysis.

Our results on nuclei of liver cells would indicate that, in nucleoplasm (the only nuclear compartment that always contains precipitates in rat parotid independently of the variant of the PA technique used (Simson and Spicer, 1975) and in fibrillar centers of the nucleolus,

Table 17. Composition of biological material. Bibliographic values (mass fraction).

	Na	Mg	P	S	Cl	K	Ca	sum	ref
Condensed chromatin	0.022	0.065	0.85	0.058	0.08	0.72		1.79	(1)
Decondensed chromatin	0.022	0.047	0.22	0.046	0.07	0.37		0.77	(1)
Cytoplasm	0.03	0.03	0.22	0.071	0.083	0.41		0.85	(1)
Nuclei	0.053	0.039	0.52	0.23	0.12	0.73	0.001	1.7	(2)
Other	0.049	0.036	0.57	0.22	0.10	0.51	0.004	1.5	(2)
Nucleus	0.006	0.02	0.26	0.052	0.11	0.47	0.006	0.92	(3)
Cytoplasm	0.01	0.021	0.3	0.056	0.081	0.41	0.004	0.88	(3)
Nuclei	0.023	0.015	0.45	0.18	0.088	0.53	0.012	1.3	(4)
Golgi	0.11	0.04	0.36	0.19	0.14	0.44	0.024	1.3	(4)
Nucleus	0.014	0.022	0.21	0.214	0.15	0.34		0.9	(5)
Cytoplasm	0.016	0.029	0.32	0.23	0.12	0.34		1.1	(5)

(1) von Zglinicki (1987) on hydrated and freeze-dried cryosections of rat liver;
(2) Somlyo (1984) on freeze-dried cryosections of rat liver;
(3) Ornberg (1989) on hydrated and freeze-dried cryosections of chromaffin cells;
(4) Gupta (1989) on hydrated and freeze-dried cryosections of intestinal cells;
(5) Zierold (1988) on hydrated and freeze-dried cryosections of rat liver.

---

the cation precipitates with PA may originate from one of the two first sources. Simson and Spicer (1975) indicated that the nature of the cation-binding material in dispersed chromatin region of the nucleus is of considerable interest. Nuclear acidic proteins have been implicated in the control of cell replication, and such anionic molecules could (loosely?) bind cations which would yield a precipitate with Sb.

The high concentration of Ca accumulated in the nucleolus and the condensed chromatin probably originates from the ionic shifts between extra- and intracellular spaces. In this case, the calcium would be tightly bound to macromolecules (nucleic acids and/or proteins).

T. von Zglinicki: Was there no external background to subtract? If there was, how was the subtraction done?
Authors: The sections were spread directly on the grids without support film; there is no external background due to support film in our spectra. The only external backgroud came from the grid that can be excited by the backscattered electrons in the specimen chamber. When using the continuum method according to Hall, the accurate substraction of the external backgroud contribution is very important. The Cliff-Lorrimer method only takes in account the characteristic peaks and their ratio and not the X-ray continuum. The two methods that we have used for continuum background substraction, taking in account the total X-ray continuum spectrum, allowed us to measure characteristic peaks.

T. von Zglinicki: Equation (5) is arbitrary, and equation (6) is surely wrong because of the missing of the light elements of the embedding medium. You will be better off with relative quantitation.
Authors: Equation (5) is not totally arbitrary. It was obtained by averaging quantitative results obtained by different authors (see Table 17). It is used for evaluating the wet-mass fractions. We agree with the fact that equation (6) must be understood as providing a way to perform relative quantification.

R.D. Leapman: What are the statistical criteria for deciding which factorial axes should be included and for deciding whether elements are correlated or anticorrelated?

Authors: Factorial axes can be considered as different orthogonal components which have to be added (with different weights) in order to reconstitute or explain the whole data set. Each of them is associated with an eigenvalue which represents the part of the total variance represented by this axis. During the course of the analysis, eigenvalues (and eigenvectors) are ranked in a decreasing order. Therefore, from a purely statistical point of view, the more important factorial axes are those with a low number (i.e., 1, 2, 3). However, from the user's point of view, the "importance" of a factorial axis is connected to its meaning. The user has to interpret factorial axes (on the basis of the associated factorial images) before deciding whether this axis is important or not for the study. In some unfavorable situations, factorial axes associated with artefacts (or noise) have a lower order than factorial axes really useful for the user.

Another problem related to your question is that of the number of factorial axes which have to be considered. Here again, an answer can be given from a statistical point of view [see for instance the answers to the questions in Bonnet and Trebbia (1992)]. However, from a practical point of view, the answer is: the user has to take into account the factorial axes he is able to interpret (on the basis of the factorial images).

Whether elements are correlated or anticorrelated is a direct result of the multivariate analysis, and can be quickly ascertained from the graphical display of the element coordinates on the factorial axes. Two elements displayed closely together are correlated and two elements far apart are anticorrelated. It should be stressed that this concept of correlation has to be associated with the concept of factorial axes or of "sources of information": within the same experiment two elements can be correlated according to a specific problem (one factorial axis) and anticorrelated according to another problem (another factorial axis). This is one of the interests of using the kind of analysis described in this paper: instead of characterizing the global correlation between two elemental maps, one is able to split this global correlation into several partial correlations, providing additional tools for the interpretation of complex situations.

R.D. Leapman: How long does a typical multivariate statistical analysis take to perform on the personal computer (PC)?

Authors: Only MSA concerning data resulting from spectrum processing are performed on a PC. Performing a Principal Component Analysis (or Discriminant Factorial Analysis) on 97 measurements (each with 7 values) takes 4 minutes with the STATITCF software running on a PC equipped with a 80286 microprocessor. An extra time of 3-4 minutes is necessary for printing the results. MSA concerning images was performed with a home-made software running on a SUN-4 workstation. It takes 30 seconds to process six 128 * 128 pixel maps.